# Highly Dispersed Alloy Catalyst for Durability

Vivek S. Murthi (Primary Contact), Elise Izzo, Wu Bi, Sandra Guerrero and Lesia Protsailo
UTC Power Corporation
195 Governor's Highway
South Windsor, CT 06042
Phone: (860) 727-2126; Fax: (860) 353-4003
E-mail: vivek.srinivasamurthi@utcpower.com

DOE Technology Development Manager: Kathi Epping Martin
Phone: (202) 586-7425; Fax: (202) 586-9811
E-mail: Kathi.Epping@ee.doe.gov

DOE Project Officer: Reginald Tyler
Phone: (303) 275-4929; Fax: (303) 275-4753
E-mail: Reginald.Tyler@go.doe.gov

Technical Advisor: Thomas Benjamin
Phone: (630) 252-1632; Fax: (630)-252-4176
E-mail: Benjamin@anl.gov

Contract Number: DE-FG36-07GO17019

Subcontractors:
Johnson-Matthey Fuel Cells, Sonning Commons, UK
Texas A&M University, College Station, TX
Brookhaven National Laboratory, Upton, NY

Project Start Date: May 1, 2007

Project End Date: June 30, 2012

## OBJECTIVES

- Develop structurally and compositionally advanced supported alloy catalyst system with loading $\leq$ 0.3 mg platinum group metal (PGM)/cm$^2$.
- Optimize catalyst performance and decay parameters through quantitative models.
- Demonstrate 5,000 cyclic hours below 80 °C with less than 40% loss of electrochemical surface area and catalyst mass activity.

## TECHNICAL BARRIERS

This project addresses the following technical barriers from the Fuel Cells section (section 3.4.4) of the Hydrogen, Fuel Cells and Infrastructure Technologies Program Multi-Year Research, Development and Demonstration Plan:

(A) Durability
(B) Cost
(C) Performance

## TECHNICAL TARGETS

**Table 1.** DOE technical targets for electrocatalysts.

| Electrocatalyst Targets | Units | DOE 2010 Target | DOE 2015 Target |
|---|---|---|---|
| Pt group metal (total content) | g/kW | 0.3 | 0.2 |
| Pt group metal (total loading) | $mg/cm^2$ | 0.3 | 0.2 |
| Mass activity @ 900mV | $A/mg_{PGM}$ at 900 mV (iR-free) | 0.44 | 0.44 |
| Specific activity | $\mu A/cm^2$ at 900 mV (iR-free) | 720 | 720 |
| Cyclic durability<br>At T ≤80°C<br>At T >80°C | <br>h<br>h | <br>5000<br>2000 | <br>5000<br>5000 |
| ECA Loss | %, percent | <40 | <40 |
| Cost | $/kW at $51.55/g | 5 | 3 |
| Electrocatalyst Support<br>mV after 400 hours @ 1.2V | mV | <30 | <30 |

**SUMMARY**

Achieving DOE's stated 5000-hr durability goal for light-duty vehicles by 2015 will require MEAs with characteristics that are beyond the current state of the art. Significant effort was placed on developing advanced durable cathode catalysts to arrive at the best possible electrode for high performance and durability, as well as developing manufacturing processes that yield significant cost benefit. Accordingly, the overall goal of this project was to develop and construct advanced MEAs that will improve performance and durability while reducing the cost of PEMFC stacks. The project, led by UTC Power, focused on developing new catalysts/supports and integrating them with existing materials (membranes and gas diffusion layers (GDLs)) using state-of-the-art fabrication methods capable of meeting the durability requirements essential for automotive applications. Specifically, the project work aimed to lower platinum group metals (PGM) loading while increasing performance and durability. Appropriate catalysts and MEA configuration were down-selected that protects the membrane, and the layers were tailored to optimize the movements of reactants and product water through the cell to maximize performance while maintaining durability. A brief summary of accomplishments from FY2008-FY2012 is provided below

**FY2008:**
The atomistic modeling work guiding the synthesis project was providing fundamental activity and durability controlling information. Preliminary samples synthesized on the project exceeded the DOE 2010 targets for mass activity when normalized to mass of Pt. However, further work is needed to achieve the PGM based mass activity targets.

**FY2009:**
Mass activities of almost 0.3 $A/mg_{PGM}$ in both RDE and subscale MEA testing have been reproduced and verified for a 30% $Pt_4IrCo_3$ and 30% $Pt_2IrCr$ that have been down-selected as the dispersed alloy catalyst

systems to be scaled-up for fuel cell demonstration. A 30% $Pt_6IrCo_7$ alloy showed a high initial mass activity, 0.73 $A/mg_{PGM}$ in RDE testing and superior durability capable of meeting the 2010 DOE targets.

Pt ML catalyst prepared using scalable chemistries and characterized by a range of techniques showed strong evidence for a core-shell structure. However, a key challenge for the core-shell catalysts was their poor durability towards potential cycling due to non-uniform Pt layer on the core structures. Various scalable methods specifically geared towards achieving uniform Pt coatings were completed.

**FY2010:**

Mass activities of ~ 0.15 $A/mg_{PGM}$ in subscale MEA testing have been reproduced and verified for a scaled-up 30% $Pt_2IrCr$ and was down-selected as the dispersed alloy catalyst system for full scale fuel cell demonstration. The $Pt_2IrCr$ alloy was chosen, over the PtIrCo alloy, based on the higher durability of Cr over Co in the alloy catalysts under the MEA fabrication process. Key barriers to overcome for the incorporation of the 30% $Pt_2IrCr$ in an MEA such as the low catalyst utilization in an MEA and the cathode catalyst layer optimization for high current density performance in a WTP fuel cell remain as the main focus under this project.

A key challenge for the core-shell catalysts was their poor durability in an MEA under operating fuel cell conditions and was extensively investigated. Application of various procedures to the $Pt_{ML}/Pd_3Co$ system such as improved reduction, acid leaching or Pd/Ir ion wash treatment of the precursor cores prior to Pt coating did not improve either MEA performance or reduce Pd dissolution. Thus, the high activity of this novel catalyst type, as indicated by RDE activity testing under more benign conditions, could not be realised in MEAs. The use of the more stable Ir cores translated to improved stability in the $Pt_{ML}/Ir$ core shell resulted in acceptable performance in MEAs. However, no cost benefit was achieved for this class of catalysts over Pt on a A/mgPGM basis.

All modeling activities under this project were completed and clearly showed the benefit of Ir and the stability it imparts to the surface Pt atoms in the ternary PtIrM alloys. Also, computational calculations played a significant role in identifying core materials and shell thickness in understanding the activity and stability benefits of core-shell catalysts.

A carbon support C4 with significant resistance to corrosion (< 30 mV loss at 1.5 $A/cm^2$, 80 °C in $H_2/O_2$) was down-selected for further scale-up of a 30% $Pt_2IrCr$ alloy catalyst, MEA optimization and durability evaluation in a subscale fuel cell.

**FY2011:**

The effects of MEA compositions and cathode GDL were studied for the scaled-up 30% $Pt_2IrCr/C$ in full-size WTP fuel cells. Short stack containing the Pt-alloy was built and its durability under an accelerated vehicle drive cycle protocol is currently under investigation. Key barriers to overcome for the incorporation of the 30% $Pt_2IrCr$ in an MEA such as low catalyst utilization in electrodes and the transition metal stability under operating conditions were investigated. It was found that MEA ink formulations and processing methods significantly impact the electrode structure in an MEA and their performance under high current density operations.

A No-Go decision was made for the core-shell catalysts due to their poor durability in an MEA under operating fuel cell conditions.

The scaled-up synthesis of a 20% $Pt_2IrCr/C4$, the down-selected catalyst on stable carbon, preliminary MEA optimization and corrosion durability testing were completed. However, their performance at high current operations was very poor due to low electrode utilizations.

**FY2012:**
The effects of MEA compositions were studied for the scaled-up 30% $Pt_2IrCr/C$ in full-size WTP fuel cells. The electrode optimization studies clearly showed that MEA ink formulations and processing methods significantly impact the electrode structure in an MEA and their performance under high current density operations. Short stack containing the 30% $Pt_2IrCr/C$ alloy catalyst was built and it's durability under an accelerated vehicle drive cycle protocol showed that the durability loss was primarily due to the transition metal dissolution (~50% loss) from the alloy. Although significant progress was made to overcome key barriers for the incorporation of the 30% $Pt_2IrCr$ in an MEA such as low catalyst utilization in electrodes, the transition metal stability under operating conditions remains a concern.

## INTRODUCTION

For the proton exchange membrane fuel cell (PEMFC) technology to become commercially viable, the production cost of the components in a fuel cell must be reduced and, more importantly, the durability of the MEA must be improved. The key requirement for cathode catalysts for PEMFCs is stability toward potential cycling under operating temperatures. In addition to showing high mass activity for oxygen reduction reaction (ORR), catalysts must survive harsh transient operation (load cycling) in a vehicle. Pt-transition metal alloys have been proposed as PEMFC cathode catalysts due to their high ORR activity and durability [1,2,3,4,5,6,7,8]. However, their benefit in an MEA has not been realized and they show poor high current density performance. Ensuring high catalyst performance in an MEA is a critical step. Current state-of-art PEM electrodes can achieve about 60-80% catalyst utilization (of the ~25% of Pt that is on the surface) using a conventional Pt catalyst. Alternatively, using Pt –transition metal alloy catalysts is a well-known approach to reduce the high cost of Pt-based catalysts and to achieve higher activity. In the case of alloy catalysts on standard supports (such as Vulcan or Ketjen Black), however, the utilization is significantly lower. The utilization of the catalyst is strongly dependent on the catalyst support structure and the design of the catalyst layer. Further, large electrochemical surface area (ECA) and transition metal losses have been observed on such catalysts in an MEA. This project focuses on two distinct approaches to the DOE 2010 durability and performance targets. The first approach is the development of conventional but high performance highly dispersed Pt alloy electrocatalyst on a carbon support. The second system utilizes a novel "Pt monolayer (ML) core-shell" approach capable of achieving very high Pt mass activities [9,10,11]. Under the former concept, the main objectives are to develop, evaluate and down-select the best alloy catalyst while simultaneously focus on lowering the catalyst loading in the MEA and designing advanced electrode structures to improve the high current density performance and durability towards cycling of the cathode by optimizing the MEA fabrication methods.

## APPROACH

To achieve the objectives on this project, UTC Power (UTCP) has teamed with Brookhaven National Laboratory (BNL), Texas A&M University (TAMU) and Johnson Matthey Fuel Cells (JMFC). The research focus and the role of all partners were reported previously [12]. BNL's role on the project focuses on the development of Pt ML "core-shell" systems on various cores including ideal surfaces such as single crystals. In addition, BNL leads our efforts to understand the effect of electronic properties, crystal structure and particle size on activity and durability of this class of electrocatalysts. TAMU focuses on development of computational atomistic models to study parameters that influence the activity and durability of core shell and dispersed catalyst systems. The overall scope of JMFC activities in the project encompasses development of (i) dispersed Pt alloy catalysts including scale-up on conventional and advanced carbon supports, (ii) novel synthesis methodologies to scale-up Pt ML core-shell catalysts and (iii) MEA optimization and fabrication. Apart from overall program management, UTCP primarily focuses on the development of advanced dispersed Pt-based binary and ternary alloy catalysts. UTCP activities also include 1) elucidation of cathode performance degradation mechanisms and development of key material characteristics that determine performance and stability, 2) development of advanced Pt-

based binary and ternary catalysts guided by molecular modeling, 3) synthesis of highly-dispersed (~2 nm metal particles) ternary alloys on advanced corrosion resistive carbon supports, 4) optimization of electrode structure through tailoring carbon support surface chemistry and ionomer-catalyst ink properties, and 5) fuel cell performance and stability testing on full-size (410 $cm^2$) MEAs, fabrication and testing of a 20-cell short stack for verification.

## ACCOMPLISHMENTS

Table 2 outlines the current status of the project with respect to the DOE technical targets. A brief description of accomplishments in order of the fiscal year are also listed below

**Table 2.** Current status of this project with respect to DOE technical targets for electrocatalysts

| Electrocatalyst Targets | Units | Current Status | DOE 2010 Target | DOE 2015 Target |
|---|---|---|---|---|
| Pt group metal (total content) | g/kW | 0.50 | 0.3 | 0.2 |
| Pt group metal (total loading) | $mg/cm^2$ | 0.40[a] | 0.3 | 0.2 |
| Mass activity @ 900mV | $A/mg_{PGM}$ at 900 mV (iR-free) | 0.17 (in MEA)<br>0.30 (in liquid cell) | 0.44 | 0.44 |
| Specific activity | $\mu A/cm^2$ at 900 mV (iR-free) | 940 (in MEA)<br>612 (in liquid cell) | 720 | 720 |
| Cyclic durability<br>At T ≤80°C<br>At T >80°C | <br>h<br>h | 2050[b,c] | <br>5000<br>2000 | 5000<br><br>5000 |
| ECA Loss | %, percent | 30[d] | <40 | <40 |
| Cost | $/kW at $51.55/g | ~26[e] | 5 | 3 |
| Electrocatalyst Support mV after 400 hours @ 1.2V | mV | 92[f] | <30 | <30 |

[a] *Based on current scaled-up 30% $Pt_2IrCr/C$ MEA; Anode/Cathode loading – 0.1/0.3 $mg/cm^2$ (PGM).*
[b] *Under an accelerated vehicle drive cycle protocol in a short stack; 40% Mass activity loss under UTC defined accelerated single-cell test after 270 hours at 70 °C and 120 hours at 80°C.*
[c] *Primary degradation mechanism in the alloy catalyst due to transition metal alloy dissolution.*
[d] *Durability data measured after 30000 cycles under UTC defined accelerated test protocol.*
[e] *5 year average PGM price $ 51.55/g (Pt = $1234.33/Troy Oz; Ir = $ 369.06/troy oz); costs not projected to high volume production.*
[f] *40 mV iR free $O_2$ performance loss at 1.5 $A/cm^2$ after 360 hours at 1.2 V.*

**FY2008:**

- Synthesized multiple batches of 40% $Pt_2IrCo$ on Ketjen Black for benchmarking.
- Modeling of the segregation behavior of dispersed binary alloys showed that most transition metals will segregate to the surface in the presence of less than a monolayer (ML) of O on the surface.

- Chemical potential calculations of the Pt dissolution reaction showed that a Pt ML on $Pd_3Co$ and Pd cores exhibit improved cyclic durability. These calculations guided the selection of core materials for core-shell catalysts.
- Dispersed catalysts with different Pt mass fractions in the $Pt_2IrCo$ alloy system were synthesized and characterized. The 30 wt% Pt catalyst was found to be the optimum within the range explored. The PtIrCo system is being further investigated with respect to variables such as composition, type of carbon support, etc.
- Pt ML catalysts on $Pd_3Co$ and Ir cores were synthesized and characterized for mass activity. When normalized to Pt content, the two catalyst systems exhibited mass activities of 1.01 and 0.57 A/mg, respectively. These values exceeded the DOE 2010 target of 0.44 A/mg.
- The scale-up of the Pt ML catalysts was initiated.

**FY2009:**

- 30% $Pt_4IrCo_3$ and 30% $Pt_2IrCr$ were down-selected as the dispersed alloy catalyst systems to be scaled-up for single cell demonstration. Mass activities of ~ 0.3 $A/mg_{PGM}$ were reproduced in both rotating disk electrode (RDE) and subscale membrane electrode assembly (MEA) testing (3x the activity of standard pure Pt catalyst).
- Dissolution trends of metal atoms other than Pt in Pt-based alloys were evaluated.
- Electronic structure and segregation properties of $Pt_3Cr$, $Pt_2IrCr$, and $Pt_2IrCo$ alloys were investigated using quantitative models to determine the most stable surface distributions.
- Surface segregation trends and stability of the surface atoms against dissolution for various shell compositions were evaluated as a function of the shell thickness for Pt ML catalysts on $Pd_3Co$ and Ir cores.
- Catalyst mass activities that surpass the DOE 2010 target for dispersed catalysts ($\geq$ 0.7 $A/mg_{PGM}$) were demonstrated in RDE testing.
- A Pt ML on $Pd_3Co$/C core-shell catalyst was scaled up from 300 mg to a 5g batch.
- MEA catalyst layer optimization activities were started.

**FY2010:**

- Down-selected a carbon (C4) that exceeds DOE's corrosion targets and verified a 30% Pt/C4 and a more active PtIrCo/C4 alloy catalyst in a subscale fuel cell which showed that PtIrM/C4 are more active and durable compared to the Pt/C4. Scale-up of a 30% $Pt_2IrCr$ alloy on C4 was completed.
- Completed the scale-up of both down-selected dispersed catalyst PtIrCr and PtIrCo for MEA optimization. Currently testing performance and durability of first trial full size MEA of 30% $Pt_2IrCr$/C.
- Modeling results show that Ir in the dispersed PtIrM (M=Co or Cr) ternary alloy catalysts imparts stability to the surface Pt atoms. The benefit of Ir in PtIrM alloy catalysts was evaluated and compared to PtM alloys.
- Sub-scale MEA catalyst layer optimization was completed to improve the ternary alloy MEA performance in $H_2$/air at high current densities with total PGM loading of 0.3 $mg/cm^2$.
- Correlation between segregation energies, activity and stability of core-shell catalysts based on their composition and surface characterization during potential cycling explains differences in the surface activity during core metal dissolution and the durability of core-shell catalysts.
- Activity and stability of $Pt_{ML}/Pd_3Co$ core-shell catalysts prepared using scalable chemistries were evaluated using both RDE and subscale fuel cell tests.

**FY2011:**

- Completed the scale-up and MEA optimization of down-selected dispersed catalyst, 30% $Pt_2IrCr/C$ for performance in a full-size fuel cell. A mass activity of 0.2 A/mg(PGM) was achieved compared to the previous status of 0.14 A/mg(PGM)
- Completed the durability testing of 30% $Pt_2IrCr/C$ in a full-size MEA under an accelerated protocol which showed 400 hrs of stability at 70C. Currently testing performance and durability of the 30% $Pt_2IrCr/C$ in a short stack.
- Durability testing of 30% $Pt_2IrCr/C$ in a short stack was initiated under an accelerated vehicle drive cycle protocol. The stack accumulated 1450 hours of uninterrupted operation at 70 °C in $H_2$/Air.
- Scaled-up a 20% $Pt_2IrCr$ alloy on the down-selected durable carbon, C4, and completed preliminary optimization of MEA for subscale fuel cell performance and stability testing in a porous plate subscale fuel cell under the DOE catalyst support corrosion protocol. A 40 mV iR free $O_2$ performance loss at 1.5 $A/cm_2$ was observed after only 360 hours of potential holds at 1.2V.
- A No-Go decision was made for core-shell catalysts based on extensive physical characterization and durability studies. Activity and stability of $Pt_{ML}/Pd_3Co$ core-shell catalysts prepared using scalable chemistries were evaluated using both RDE and subscale fuel cell tests. Higher temperature and more concentrated electrolyte contribute to Pd dissolution and are substantially more damaging than room temperature RDE testing.

**FY2012:**

- Completed the scale-up and MEA optimization of down-selected dispersed catalyst, 30% $Pt_2IrCr/C$ for performance at high current densities in a full-size fuel cell. A mass activity of 0.17 A/mg (PGM) was achieved compared to the previous status of 0.14 A/mg (PGM) with a 53 mV improvement in performance at $1A/cm^2$ in $H_2$/Air
- Completed the durability testing of 30% $Pt_2IrCr/C$ in a short stack under an accelerated vehicle drive cycle protocol. The stack accumulated 2050 hours of uninterrupted operation at 70 °C in $H_2$/Air. Completed stack teardown to understand degradation mechanism for $Pt_2IrCr$ alloy: primary durability loss in the alloy catalyst was due to transition metal dissolution.

**RESULTS**

A summary of results in order of the fiscal year is given below

**Molecular Modeling**

**2008:**

There were two topics studied in FY2008. The first dealt with quantifying segregation energies to study the stability of dispersed Pt alloys. For various binary Pt alloys, the Vienna Ab-Initio Simulation Package (VASP) was used to calculate the thermodynamic favorability for Pt to remain on the surface of the alloy. The simulations were carried out under assumed conditions of vacuum and in the presence of a ML of oxygen on the surface. In vacuum, it was observed that Pt remained on the surface for most transition metals [13]. In contrast, with as little as a quarter ML of oxygen on the surface, the transition metal segregated to the surface in most cases. This is shown in Table 3 which contains segregation energies in eV for the vacuum and O ML case for four different alloys. Note that negative segregation energy signifies stable Pt on the surface. From Table 3, it is seen that only in the presence of a non-transition metal like Ir, Pt exhibits stability against segregating to the interior of the particle. Even in the case of Ir, the relatively low energies signify a borderline stability.

**Table 3.** Segregation Energies in Vacuum and in the Presence of 0.25 ML of O on the Surface

| $E_{seg}$ (eV) | $Pt_3Ir$ (111) | $Pt_3Co$ (111) | $Pt_3Fe$ (111) | $Pt_3Ni$ (111) |
|---|---|---|---|---|
| Under 0.25 MLof O | -0.54 | 0.14 | 0.45 | 0.20 |
| Vacuum | -0.54 | -0.61 | -0.41 | -0.38 |

The modeling results with Ni, Co and Fe agree with published low energy electron diffraction (LEED) data measured [7,14].

For core-shell structures, VASP was used to study the chemical potentials for the Pt dissolution reaction. These data are presented in Figure 1.

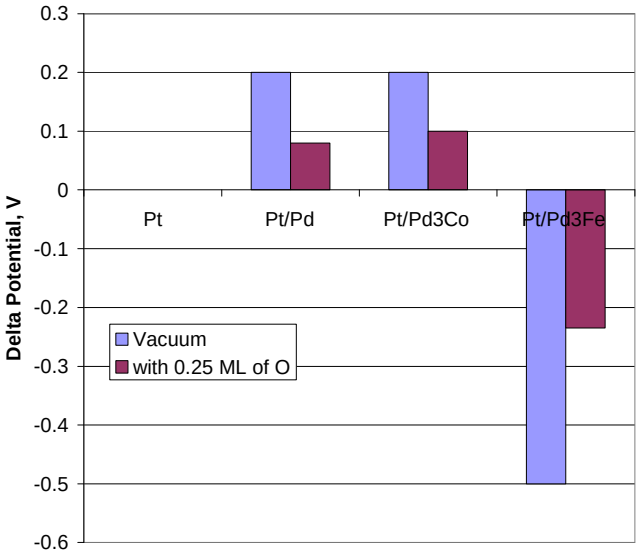


**Figure 1.** Difference in Equilibrium Potential for Pt Dissolution on bare Pt and different Core-Shell Pt ML Catalysts (A negative delta potential signifies a less stable catalyst compared to pure Pt.)

The delta potential presented in Figure 1 represents the difference in the equilibrium potential for Pt dissolution between the core shell structure and pure Pt. A negative potential difference indicates reduced stability with respect to the baseline pure Pt. As seen from Figure 1, a Pt ML on $Pd_3Co$ and Pd show improved stability with and without oxygen adsorption. These calculations were used to support our core shell synthesis and characterization work.

**2009:**

The main topic that was studied this year was calculation of adsorption energies of atomic oxygen on segregated Pt-skin and non-segregated $Pt_3M$ and $Pt_2IrM$ (M= Cr, Fe, Co, and Ni) alloy surfaces. The results indicate that in non-segregated $Pt_3M$ alloy surfaces, the adsorption energies of 0.25 ML atomic oxygen follows the trend Pt < $Pt_3Ni$ < $Pt_3Co$ < $Pt_3Fe$ which is exactly opposite of the trend observed in segregated $Pt_3M$ surfaces. To investigate the origin of the differences between the two types of surfaces, d-band center and d-band filling were calculated along with their main geometric parameters. Table 4 illustrates that the shift of the d-band center for $Pt_3M$ and Pt-skin is very similar, and so is filling of the d-band center. This indicates that electronically, the Pt atoms on skin surfaces differ little from those on the non-segregated alloy surface. It was found that in non-segregated surfaces, electronic effects dominate because the 3-d metals are oxophilic. In contrast, the Pt segregated surfaces are affected by both electronic and geometric effects. In addition, the electronic structure of segregated and non-segregated $Pt_3M$ and PtIrM alloys (M= Cr, Fe, Co, and Ni) were also correlated to adsorption strength and surface

stability against dissolution. Examination of the segregation trends of the $Pt_2IrCr$ alloy reveals that the ordered alloy surface is electrochemically more stable than Pt-skin surfaces against Pt dissolution. The most favorable Pt skin surface has a composition of $PtIrCr_2$ in the subsurface. However, the d-band center of the non-segregated surface was found to be -2.3 eV, almost the same as that of the segregated Pt-skin surface (-2.31 eV), denoting similarity of these two electronic configurations. [15]

In the core-shell catalyst concept, the stability and segregation trends of Pt ML on various core materials such as Pd-containing metal cores, IrCo alloyed cores, and different compositions of $Ir_xCo_y$ cores were investigated as a function of several parameters including (a) composition of the Pd in the 2nd layer, (b) the adsorption site for atomic oxygen and (c) the Pt-shell thickness. It is observed that the 1-layer shells offer slightly enhanced resistance for the Pt atoms to dissolve from the surface relative to 2 layer shells, as revealed by the positive potential shift relative to those in a pure Pt (111) surface both under vacuum and in 0.25 ML oxygen. The relative stability decreases for the 2-layer shell, though Pt atoms are still more stable than in pure Pt (111). Based on the above results it was observed that the Pd core enhances the stability of the atoms in the 1-layer shell and the benefit of the Pd core is reduced when the shell thickness increased. [16]

**Table 4.** Calculated Geometric and Electronic Properties of Pt (111) and $Pt_3M$ (111) Surfaces [a]

| | interlayer distance (Å) | | | |
|---|---|---|---|---|
| | $d_{12}$ | $d_{23}$ | $\varepsilon_d - \varepsilon_F$ (eV) | $f$ (%) |
| Pt (111) | 2.323 | 2.283 | – 2.40 | 90.1 |
| $Pt_3Fe$ (111) | 2.231 | 2.263 | – 3.11 | 89.8 |
| $Pt_3Fe$ – Pt skin | 2.303 | 2.235 | – 3.06 | 89.3 |
| $Pt_3Co$ (111) | 2.221 | 2.257 | – 3.02 | 89.5 |
| $Pt_3Co$ – Pt skin | 2.241 | 2.169 | – 2.98 | 89.3 |
| $Pt_3Ni$ (111) | 2.236 | 2.277 | – 2.51 | 89.6 |
| $Pt_3Ni$ – Pt skin | 2.238 | 2.219 | – 2.46 | 89.3 |

[a] $d_{12}$ and $d_{23}$ refer to the distance between the first and second layers and between the second and the third layers, respectively; $\varepsilon_d - \varepsilon_F$ refers to the d-band center of the surface Pt atoms referenced to the Fermi level; and $f$ is the filling of the d-band of the surface Pt atoms.

**2010:**

The main topic that was studied this year was calculation of activity and stability of PtIrM ternary alloys based on surface segregation, Bader charge, d-band center analysis of Pt and potential shifts in the dissolution potential for Pt in these alloys. It was previously reported that, in $Pt_3M$ binary alloys, electronically the Pt atoms on skin surfaces differ little from those on the non-segregated alloy surface. In contrast, incorporating Ir into the bimetallic alloy increases the tendency of Pt-skin formation and enhances the stability of the alloy systems. Since Ir has a smaller atomic volume and higher surface energy than Pt, a much stronger Pt segregation trend is expected in the ternary PtIrM alloy system. The calculated segregation energies (in vacuum) of -2.90 eV for $Pt_2IrCo$, -2.10 eV for $Pt_4IrCo_3$, and -1.60eV for $Pt_6IrCo_7$, suggests that the presence of Ir reduces the lattice mismatch between Pt - Co and favors the formation of a Pt monolayer skin surface. However, the trend to form Pt-skin in PtIrCr alloys is lower compared with the corresponding PtIrCo alloy surfaces. Bader charge analysis (shown in Table 5) on the Pt-skin surfaces, indicates that Pt surface atoms have an excess of electrons in their valence shell and a

deficit of electron charge on the subsurface atoms (Ir, Co and Cr), which suggests a higher ORR activity for these alloy catalysts compared to a pure Pt (111).

**Table 5.** Average valence charge for surface and subsurface atoms of $Pt_xIr_yM_z$ systems.

| Geometry | Charge surface Pt atoms | Charge subsurface Co/Cr atoms |
|---|---|---|
| pure Pt(111) | -0.05 | N/A |
| $Pt_2IrCr$ (Pt-skin) | -0.25 | 1.22 |
| $Pt_4IrCr_3$ (Pt-skin) | -0.25 | 1.11 |
| $Pt_6IrCr_7$ (Pt-skin) | -0.40 | 0.77 |
| $Pt_2IrCo$ (Pt-skin) | -0.14 | 0.57 |
| $Pt_4IrCo_3$ (Pt-skin) | -0.25 | 0.43 |
| $Pt_6IrCo_7$ (Pt-skin) | -0.24 | 0.37 |

Ir also induces a larger average d-band center shift for the Pt-skin surfaces on PtIrM compared to $Pt_3M$. For comparison, the average d-band center shift for Pt-skin on $Pt_2IrCo$ and $Pt_3Co$ is -2.23 eV and -2.18 eV respectively. This negative shift is due to the presence of Ir in the subsurface and thereby modifying the electronic structure of the surface Pt atoms. A *d*-band center shift to more negative values indicates that the Pt-skin surface is less reactive and hence, certain repulsion towards oxygenated species is expected due to the negative charges located on the surface atoms. The calculated *d*-band centers relative to the Fermi level also show a shift towards lower energies in the alloys as a function of the amount of Ir in the alloy as shown in Figure 2 for PtIrCo alloys.

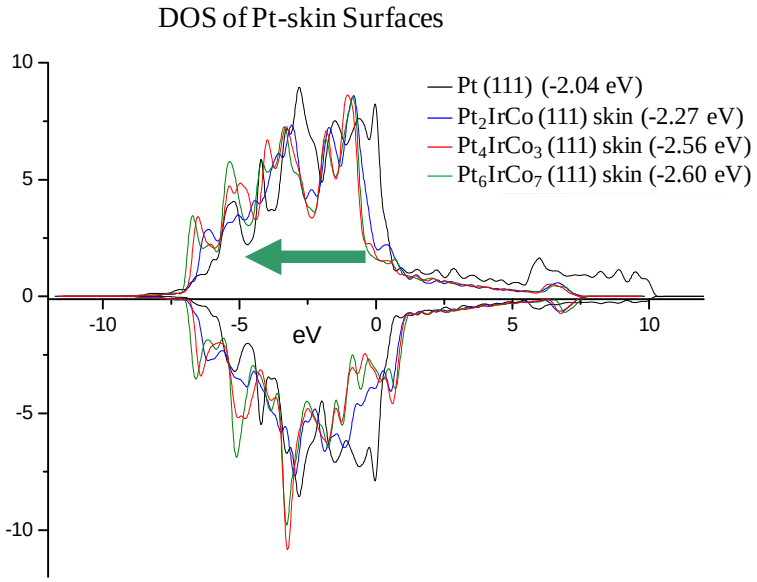


**Figure 2.** Calculated *d*-band centers relative to the Fermi level for the various Pt-skin/PtIrCo alloy surfaces as a function of the amount of Ir in the alloy.

The electrochemical stability of Pt atoms shown in Table 6 indicates that the Pt atoms are more stable on the alloy surfaces than on pure Pt (111) surfaces as shown by the positive shift in potentials on surfaces covered with 1/8 ML of O. The maximum values found for an intermediate amount of Ir suggests that further lowering the amounts of Ir in the alloy compositions may result in less stable surfaces due to the large lattice mismatch between Pt and transition metal atoms [17].

**Table 6.** Electrochemical stability of Pt atoms on Pt-skin/PtIrM (M=Co or Cr) alloy surfaces relative to Pt (111) surfaces on surfaces covered with 1/8 ML of O.

| System | $\mu_{Pt}$ (eV) | $\Delta\mu$ (eV) | $\Delta U$ (V) (under 1/8 ML O) |
|---|---|---|---|
| Pt(111) | -6.64 | 0 | 0 |
| Pt/$Pt_2IrCo$(111) | -7.00 | -0.36 | 0.18 |
| Pt/$Pt_4IrCo_3$ (111) | -7.04 | -0.40 | 0.20 |
| Pt/$Pt_6IrCo_7$ (111) | -6.91 | -0.27 | 0.14 |
| Pt/$Pt_2IrCr$(111) | -7.63 | -0.99 | 0.5 |
| Pt/$Pt_4IrCr_3$ (111) | -7.21 | -0.57 | 0.29 |
| Pt/$Pt_6IrCr_7$ (111) | -7.67 | -1.03 | 0.52 |

In the core-shell catalyst concept, the activity and stability trends of Pt ML on various Pd-containing metal cores such as $Pd_3Co$, $Pd_3Cr$ and $Pd_3Ti$ were investigated. Adsorption energies of OH, O and $H_2O$ suggest that both Pt/$Pd_3Co$ and Pt/$Pd_3Cr$ are more active than a pure Pt although the Pt/$Pd_3Co$ shows the weakest adsorption energies. The electrochemical stability investigation of Pd, Co and Cr in these core-shell catalysts shows that Pd, Co and Cr are more stable in the alloy cores than in their pure state and their stability towards leaching follows the order Pd > Co > Cr. Based on these activity and stability results, $Pt_{ML}/Pd_3Co$ is estimated to be a more favorable core-shell system for ORR compared to Pt/$Pd_3Cr$.

**2011:**

It was previously reported that incorporating Ir into the bimetallic $Pt_3M$ alloy increases the tendency of Pt-skin formation and enhances the stability of the alloy systems [12]. The main topic that was studied this year was calculation of activity and stability of PtIrM ternary alloys based on experimentally found structures including surface segregation trends, Bader charge and D-band center analysis of Pt. Previously, the change in the composition of the Pt, Ir and Co in a 30% $Pt_7IrCo_7$/C as a function of cycling and the corresponding mass activity from RDE experiments were reported. A substantial loss of Co and Ir within the first 5000 potential cycles results in a composition equivalent to that of a $Pt_3IrCo$. The role of Ir and Co on the surface properties of two structures: $Pt_8IrCo_3$ (that resulted after acid exposure) and $Pt_{11}IrCo_4$ (composition obtained after 5000 cycles) alloys were studied by DFT calculations.

The role of Ir and Co on the surface properties of PtIrCo alloys was studied by a comparative analysis for the $Pt_8IrCo_3$ and $Pt_{11}IrCo_4$ systems using 2 different 5-layer distribution structure models as shown in figure 3. The results show that the most stable structures for $Pt_8IrCo_3$ are the structures with 1-layer of Pt skin surface followed by the two-layer Pt skin surfaces. In both cases, the Pt-skin layers are more stable than the un-segregated structure. However, differences among different structures also depend critically on the subsurface composition. For example, the most stable 1-layer Pt skin surface has a second layer of $Pt_3Co$ which is slightly more favorable than a PtCo in the second layer. Similar results were obtained for the $Pt_{11}IrCo_4$ system where the most favorable second layer composition is PtCo, followed by $Pt_3Co$, and the movement of Ir from 4$^{th}$ to the 3$^{rd}$ layer does not affect the results. In summary, for the cycled and acid-treated structures, the single-layer Pt-skin surfaces are the most stable. However, the two-layer Pt-skin surfaces may be formed and are thermodynamically more favorable than the non-segregated

structures. Co atoms tend to be in the 2nd and 3rd layers, and Ir atoms tend to be in the core, together with 4th and 5th layer Pt atoms that do not show a trend to segregate towards the top surface.

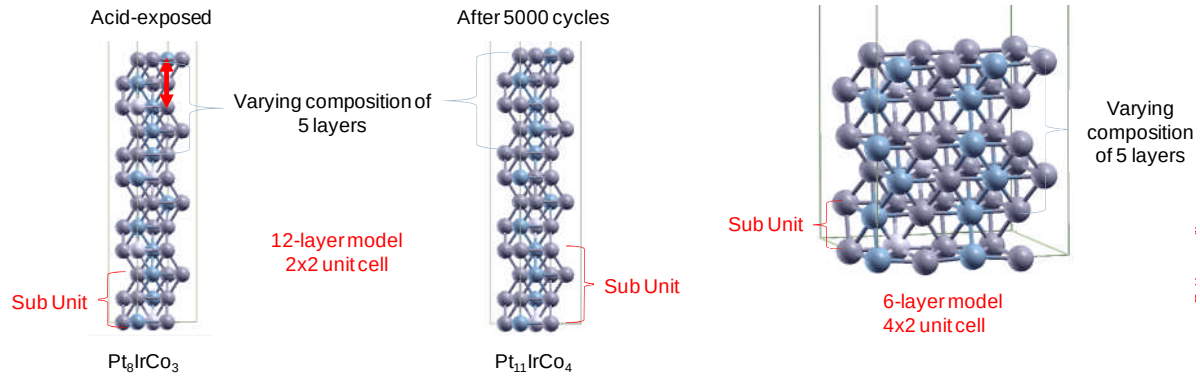


**Figure 3.** The (a) 2x2 and (b) 4x2, slab model used to study segregation in $Pt_8IrCo_3$ and $Pt_{11}IrCo_4$ systems. The first five layers are used to study atomic redistribution after leaching. The optimized lattice constants are 3.853 Å for $Pt_8IrCo_3$ and 3.851 Å for $Pt_{11}IrCo_4$.

The activity and stability of the 30% $Pt_7IrCo_7$/C after potential cycling were studied and Table 7 shows the electrochemical stability values for the $Pt_{11}IrCo_4$ (composition after 5000 cycles) structure in vacuum which shows that the stability of the cycled alloy surface is higher than that of the 2-layer skin from $Pt_2IrCo$ and comparable to that of the single layer skin of $Pt_3Co$ surfaces as shown by their electrochemical potential relative to a Pt (111) surface.

**Table 7.** Electrochemical stability of Pt surface atoms Pt surface atoms in 2-layer alloy relative to clean Pt (111) surfaces.

| System | $\mu_{Pt}$ (eV) | $\Delta\mu$ (eV) | $\Delta U$ (V) |
|---|---|---|---|
| Pt(111) | -6.98 | 0 | 0 |
| $Pt_3Co$ (111) single layer Pt-skin | -7.22 | -0.24 | 0.12 |
| $Pt_2IrCo$(111) 2-layer Pt-skin | -7.12 | -0.14 | 0.07 |
| $Pt_{11}IrCo_4$(111) 2-layer Pt-skin | -7.23 | -0.25 | 0.13 |

The average charge (based on a Bader charge analysis) of the first four layers of the $Pt_{11}IrCo_4$ indicates a charge transfer from the Co subsurface atoms to the Pt atoms in the 2nd layer and to the Ir atoms in the 3rd layer and that the charge of the surface Pt atoms remains very similar to that on the pure Pt (111) surface suggesting an increased activity of the $Pt_{11}IrCo_4$ surface. Similar results are also obtained from the analysis of the density of states calculations which suggest enhanced reactivity of the surface Pt layer (d-band center shifted in the direction of the Fermi level). Weak adsorption of O and OH intermediates are also observed compared to Pt (111) surfaces which confirms the higher activity of the $Pt_{11}IrCo_4$ alloy surface. Furthermore, the electrochemical stability values for the $Pt_{11}IrCo_4$ structure with 0.25ML of adsorbed oxygen (Table 8) shows a decrease in surface stability of the cycled alloy surface. However, the stability is still comparable to those on pure Pt (111) surfaces. These findings support the activity and stability of the 30% $Pt_7IrCo_7$/C observed experimentally [18]

**Table 8.** Electrochemical stability of Pt surface layer under 0.25 ML of adsorbed O in 2-layer alloy surface shown in Table 1 relative to pure Pt(111) surfaces

| System | $\mu_{Pt}$ (eV) | $\Delta\mu$ (eV) | $\Delta U$ (V) |
|---|---|---|---|
| Pt(111) | -6.26 | 0 | 0 |
| $Pt_3Co$ (111) single layer Pt-skin | -6.55 | -0.29 | 0.15 |
| $Pt_2IrCo$(111) 2-layer Pt-skin | -6.32 | -0.06 | 0.03 |
| $Pt_{11}IrCo_4$(111) 2-layer Pt-skin | -6.14 | 0.12 | -0.06 |

**Dispersed Pt Alloy Catalyst**

**2008:**

The activity and durability of the dispersed alloy catalyst depends on many factors including composition of alloy, particle size, particle dispersion uniformity, type of carbon used, etc. In a previous project, UTC showed that the durability of PtIrCo ternary alloys was "best in class" [8]. To further improve the mass activity of this ternary alloy, the impact of Pt mass fraction on electrochemical activity was investigated. Various samples of $Pt_2IrCo$ with mass fraction of Pt between 20 to 40 percent were investigated using the rotating disk electrode (RDE) method. Physical characterization data including X-Ray diffraction (XRD) and transmission electron microscopy (TEM) thus far have shown that lowering the Pt mass fraction lead to smaller particles and less agglomeration. Electrochemical RDE testing has yielded higher electrochemical surface area (ECA) and higher mass activity. An optimum loading of 30 wt% of Pt in $Pt_2IrCo$ exhibited an activity almost two times higher than 20 and 40 weight percent samples (0.28 $A/mg_{Pt}$ compared to 0.15 $A/mg_{Pt}$). These data are shown in Figure 4. The 30 weight percent catalyst is currently being used to fabricate MEAs to quantify performance and durability in a subscale cell. The synthesis method and the impact of the composition of Pt, Ir and Co and other transitional metals instead of Co are currently being investigated to further improve mass activity.

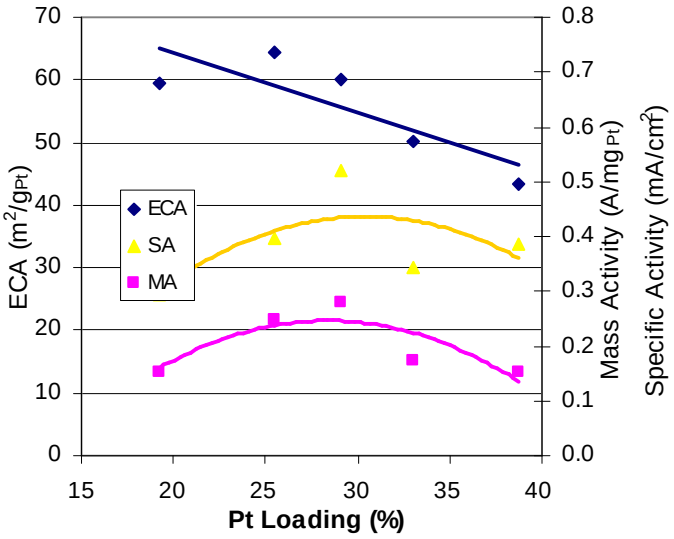


**Figure 4.** ECA, Mass Activity and Specific Activity Dependence as a Function of Pt Mass Fraction for $Pt_2IrCo$ Cathode Catalyst (The support for all the samples was Ketjen Black.)

To further improve the durability of the Pt alloys being synthesized on this project, deposition of Au clusters is being investigated. Sasaki *et al.* showed using X-ray absorption spectroscopy (XAS) that the Au clusters improve cycling stability by raising the potential for oxide formation on the surface of the Pt [19]. As a potential method to improve the durability of alloys being synthesized on this project, the effect of the deposition of Au on carbon supported large Pt particles was studied. JMFC synthesized 8 nm diameter Pt particles on Ketjen Black which were subsequently treated with 0.6 ML of Au by BNL. The Pt catalysts with and without Au were tested for electrochemical activity and durability by potential cycling in an RDE experiment. In the cycling experiment, the potential varied from 0.95-0.7 V in a square wave format with 30 second holds at each of the voltages. For both the electrodes, with and without Au deposited, the electrochemical surface area and the catalyst activity decreased with increasing cycle number. However, the loss of catalytic activity was suppressed in the Au deposited electrode. The activity of the catalyst decreased by approximately 20 mV in 30,000 cycles and 37 mV in 10,000 cycles for the cases with and without Au deposition, respectively.

**2009:**

Figure 5a and 5b show the ECA and PGM mass activity vs. potential stability during cycling test respectively obtained from RDE testing for a 30% $Pt_4IrCo_3$ (DOE 48), a 30% $Pt_2IrCr$ (DOE 52) and a 30% $Pt_6IrCo_7$ (DOE 59-1) ternary alloys compared to a commercial TKK 46.4% Pt catalyst. It should be noted that $Pt_6IrCo_7$ was synthesized in an effort specifically to reduce the total platinum group metal (PGM) content in the catalyst nanoparticles. The change in ECA with number of potential cycles (Figure 5a) shows that the 30% $Pt_4IrCo_3$ and 30% $Pt_2IrCr$ ternary alloy compositions are more resistant to loss of electrochemical area compared to the commercial Pt/C. Preliminary results on the 30% $Pt_6IrCo_7$ alloy catalyst shows a high initial mass activity (~ 0.72 A/mg of PGM) and ECA (~ 91 $m^2/g_{Pt}$). This exceeded previously reported mass activities for state-of-the-art cathode catalysts by approximately 3.5x. The durability of this electrocatalyst under accelerated potential cycling test was 0.3 $A/mg_{PGM}$ after 20,000 cycles. This is approaching the DOE 2010 initial mass activity targets for catalysts.

(a)

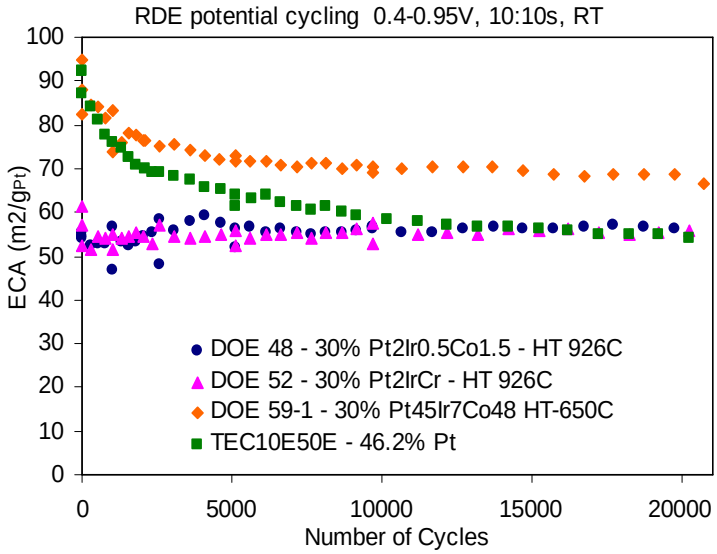


(b)

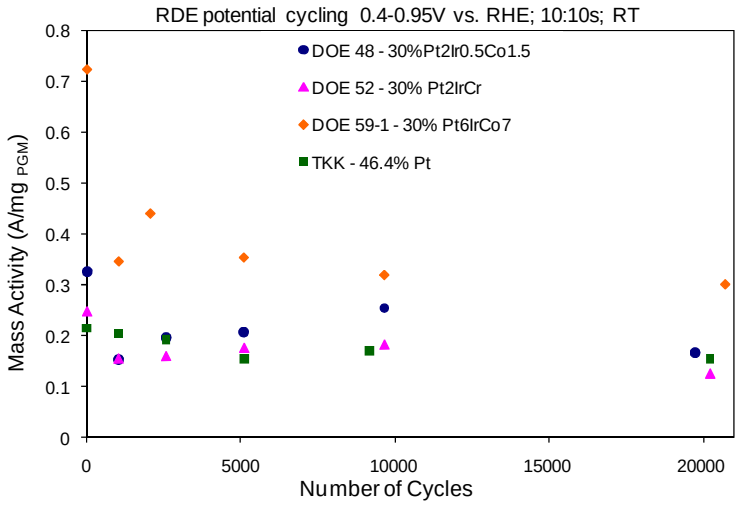


**Figure 5.** (a) ECA decay and (b) PGM mass activity decay, as a function of number of potential cycles on various PtIrM (M = Co and Cr) ternary alloy catalysts obtained from RDE testing in 0.1 M $HClO_4$ at room temperature between 0.4 (10 sec) and 0.95 (10 sec) V vs RDE.

Figure 6 shows the internal resistance (iR) corrected fuel cell performance curves in $H_2/O_2$ for the 30% $Pt_4IrCo_3$ (DOE 48) and 30% $Pt_2IrCr$ (DOE 52) compared to a standard Gore 57 Pt/C (G57) before and after 30,000 potential cycles. At the beginning of life, the Pt/C shows higher performance compared to the PtIrM ternary alloy catalysts. It should be noted that initial Pt loading in commercial MEA is about two times of that of the alloy MEAs used in this project. After 30,000 cycles, the end of life performance (EOL) for the Gore 57 Pt/C catalyst is lower than the alloy catalysts in spite of unfavorable loading in alloy MEA. This trend closely follows the results obtained from potential cycling in RDE as shown in Figures 5a and 5b. The benefit of the Ir containing ternary alloy catalysts are evident from the mass activity and ECA under potential cycling shown in Figures 7a and 7b respectively. The initial mass activity obtained for the 30%$Pt_2IrCr$ (DOE 52) alloy catalyst is ~ 0.39 $A/mg_{Pt}$ (0.28 $A/mg_{PGM}$) and EOL activity is 0.22 $A/mg_{Pt}$(0.16 $A/mg_{PGM}$). After 30,000 cycles, the mass activity of Gore standard Pt/C is less than 0.1 $A/mg_{Pt}$, a loss

of more than 50% whereas the PtIrM ternary alloy catalysts show much lower loss in mass activity (~ 30%).

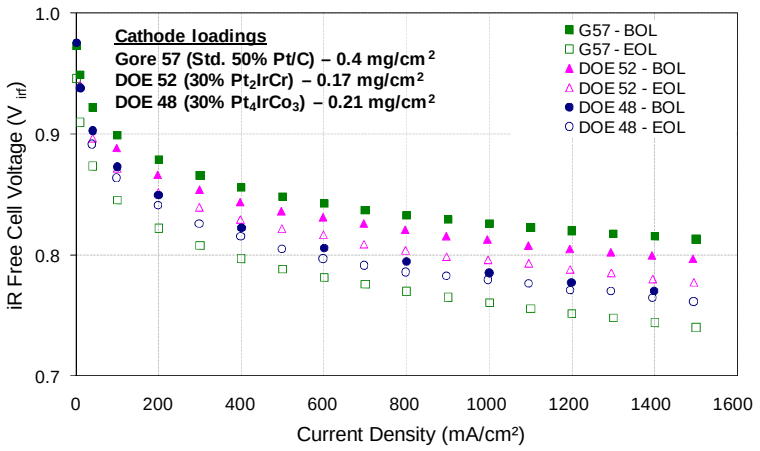


**Figure 6.** iR corrected fuel cell polarization curves in $O_2/H_2$ at 80°C; 100% relative humidity; 150 kPa, for the PtIrM ternary alloys compared to a state-of-art Pt/C MEA before and after 10s – 10s square wave potential subjected between 0.4 – 0.95 V for 30,000 cycles.

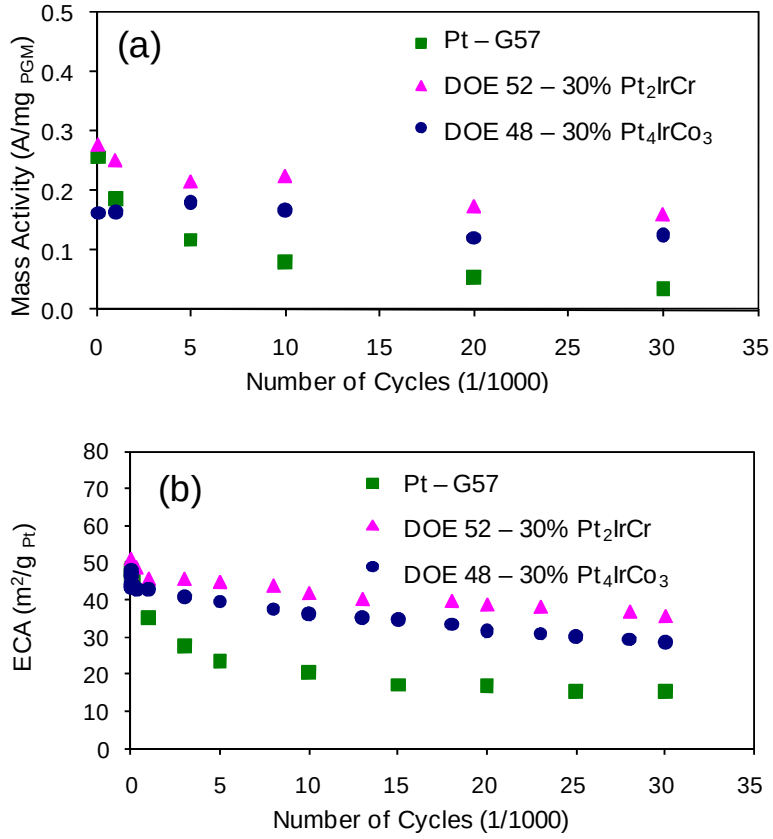


**Figure 7.** (a) PGM mass activity decay and (b) ECA decay, as a function of number of potential cycles on two PtIrM (M = Co and Cr) ternary alloy catalysts obtained in MEA testing.

**2010:**

Many factors such as structure, particles dispersion, particle size, type of carbon support used etc, influence the electro-catalytic activity of Pt and Pt alloy nanoparticles. Previously, within this project a 30 wt% $Pt_2IrCo$ and a 30% $Pt_4IrCo_3$ exhibited an activity almost two times higher than pure Pt based on RDE and MEA testing. The Ir containing ternary alloy catalysts also showed more durability in both their electrochemical active area (ECA) and mass activity (MA) under potential cycling which show much lower loss (~30% ECA and MA) compared to the standard Gore Pt/C which showed ~50% loss. Based on these results the PtIrM ternary alloys were down-selected for further development [12]. In the past years, a significant amount of effort was focused towards scale-up of a large size batch (200 g) of the down-selected ternary alloys 30% $Pt_4IrCo_3$ and 30% $Pt_2IrCr$, development and optimization of the cathode catalyst layer in an MEA of PtIrM (M= Co, Cr) alloy catalysts to improve the catalyst utilization in an MEA keeping low PGM loading and enabling good performance at high current densities. This involved MEA iterations to identify key parameters such as catalyst ink formulations and ionomer content, to achieve optimum cathode catalyst layer capable of achieving good fuel cell performance operating on not only $H_2/O_2$ but also on $H_2$/Air at high current densities.

Figure 8a shows the fuel cell performance curves in $H_2$/Air for an optimized and un-optimized 30% $Pt_2IrCr$/C MEA in a sub-scale size (25 $cm^2$) solid plate fuel cell operating at 80 °C, 100% RH and 50 kPa backpressure compared to a commercial Gore 5710 Pt/C MEA. It should be noted that the Pt loading in the commercial MEA is about two times of that of the alloy MEAs used in this project. The internal resistance for the PtIrCr MEA is also higher than the Gore 5710 MEA resistances which arise from differences in the membrane thickness and the catalyst layer fabrication process. The initial mass activity obtained for the alloy catalyst in the optimized and un-optimized MEA were 0.14 and 0.156 $A/mg_{PGM}$ respectively compared to a mass activity of 0.17 A/mg PGM observed for the commercial Pt/C MEA. This observed low activity is attributed to the low utilization of the catalyst in the MEA as seen by their low ECA of ~30 $m^2/g$. However, a clear evidence of improvement for high current density performance in $H_2$/Air in a solid plate fuel cell is observed from these catalyst layer optimization steps. The 30% $Pt_2IrCr$ ternary alloy MEA optimized for solid-plate fuel cell performance was also verified in a full size UTC's WTP fuel cell operating at 65 °C, 100%RH and 0 kPa backpressure. Figure 8b shows the internal resistance (iR) corrected fuel cell polarization curves obtained in $H_2/O_2$ for the 30% $Pt_2IrCr$ in the WTP fuel cell. Our results shows clear evidence that lower catalyst loading of 0.2mgPt/$cm^2$ in MEA's can achieve high initial performances, although lower than a commercial Pt/C which has 0.4 mg Pt/$cm^2$ in the cathode, in both solid plate and a WTP fuel cell. Our preliminary investigation into MEA fabrication process suggests that different ink formulations can significantly increase both mass transport properties and kinetic performance of alloy catalysts. Further optimization steps are currently being pursued to improve the MEA fabrication process and utilization of the catalyst in the MEA.

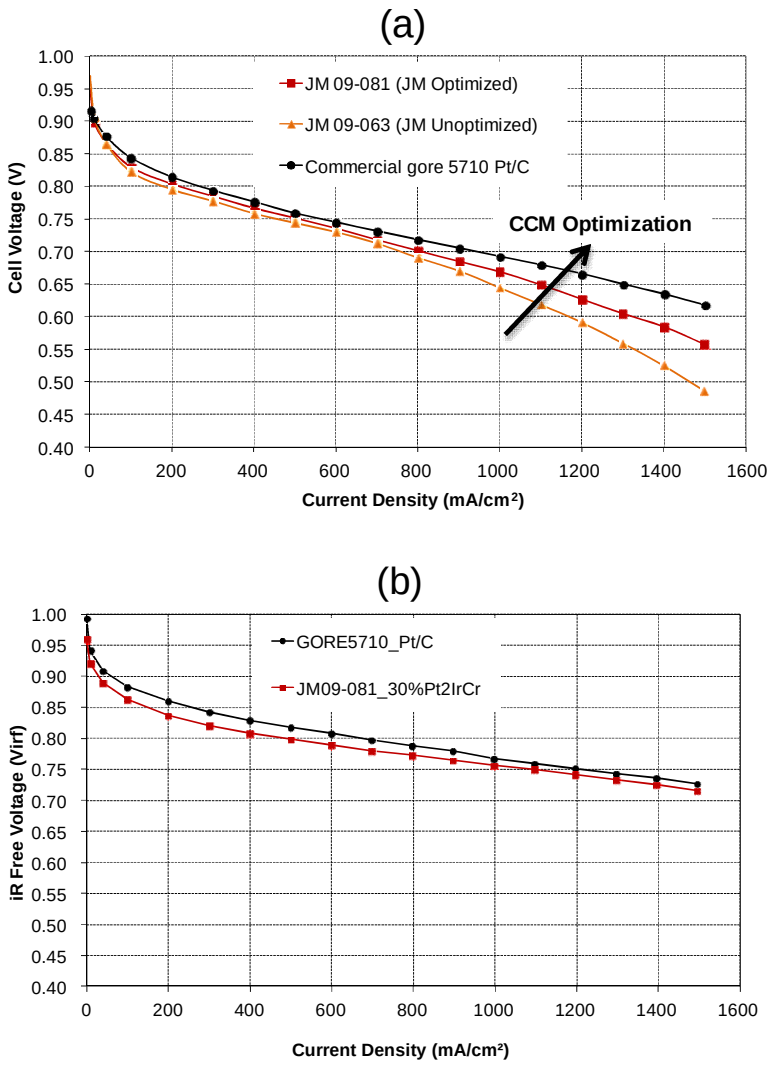


**Figure 8.** Fuel cell polarization curves in (a) $H_2$/air at 80°C in a solid plate fuel cell at 100% RH and 150 kPa backpressure for an optimized and un-optimized $Pt_2IrCr$ ternary alloy catalyst MEA compared to a state-of-art Pt/C MEA and (b) $H_2/O_2$ at 65°C in a WTP cell at 100% RH and 100 kPa backpressure, for an un-optimized $Pt_2IrCr$ ternary alloy catalyst MEA compared to a state-of-art Pt/C MEA.

## Durable Carbon Support

The main focus of this task was to explore alternate durable carbon supports capable of withstanding high voltage spikes relevant for automotive applications. Several carbon supports from a number of vendors available both commercially and under proprietary agreements were tested by subjecting pellets of these carbon samples to a constant potential hold of 1.4 V in 0.5 M $H_2SO_4$ at 80 °C for 5 hours. Based on the weight loss after the 5 hour potential hold and also on the carbon loss as $CO_2$, carbon supports C4 and modified C3 were down-selected for further testing in fuel cells under the DOE 2008 carbon corrosion protocol outlined in Table 9.

**Table 9.** DOE 2008 Carbon corrosion protocol.

| **Cycle** | Hold at 1.2 V for 24h; run polarization curve and ECA; repeat for total 400h. Subscale cell 25 $cm^2$ | |
|---|---|---|
| **Total time** | Continuous operation for 400 h | |
| **Diagnostic frequency** | 24 h | |
| **Temperature** | 80ºC | |
| **Relative Humidity** | Anode/Cathode 100%/100% | |
| **Fuel/Oxidant** | Hydrogen/Nitrogen | |
| **Pressure** | 100 kPa absolute | |
| **Metric** | **Frequency** | **Target** |
| **$CO_2$ release** | On-line | **<10% mass loss** |
| **Catalytic Activity** | Every 24 h | <60% loss of initial catalytic activity |
| **Polarization curve from 0 to >1.5 $A/cm^2$** | Every 24 h | <30mV loss at 1 $A/cm^2$ in $O_2$ |
| **ECA/Cyclic Voltammetry** | Every 24 h | <40% loss of initial area |

BOL performance obtained from a water transport plate subscale fuel cell testing at 80 °C, 100% RH under $H_2/O_2$ at zero backpressure for both the 0.2 $mg_{Pt}/cm^2$ Pt/C4 and Pt/modified C3 (low surface area carbons) show lower performance than that of a standard Gore Pt/C. However, their performances after the 1.2 V potential hold tests show considerable differences. Figure 9a shows the performance loss in $H_2/O_2$ at BOL and EOL after a single potential hold test at 1.2 V for 60 h for the Gore 5710 Pt/C. Figure 9b and c show the performance loss in $H_2/O_2$ at BOL and EOL after 24hr, 1.2V potential holds for Pt/modified C3 and Pt/C4, respectively. Also shown is the number of hours of potential hold at EOL which was determined by the performance loss at 1 $A/cm^2$ in $O_2$. Hence, there was a difference in the number of hours to reach EOL for the three catalysts. The total carbon loss during the 1.2 V potential hold as $CO_2$ was measured using an on-line NDIR spectrometer. Table 10 summarizes the performance loss in $O_2$ along with ECA loss, total resistance change in the MEA and % carbon loss from the cathode for the results shown in figure 9 for the Gore 57 Pt/C, Pt/modified C3 and Pt/C4. The carbon loss was higher than expected for the performance loss seen, and could have some contributions from the GDLs or water transport plates. The most important result in this table was performance loss at 1 $A/cm^2$. The 30%Pt/C4 only had 27 mV loss after the full test, 17 different 24h potential holds at 1.2V. All other carbon tested in the WTP subscale hardware had over 30 mV loss in performance after only 3-5 potential holds.

(a)

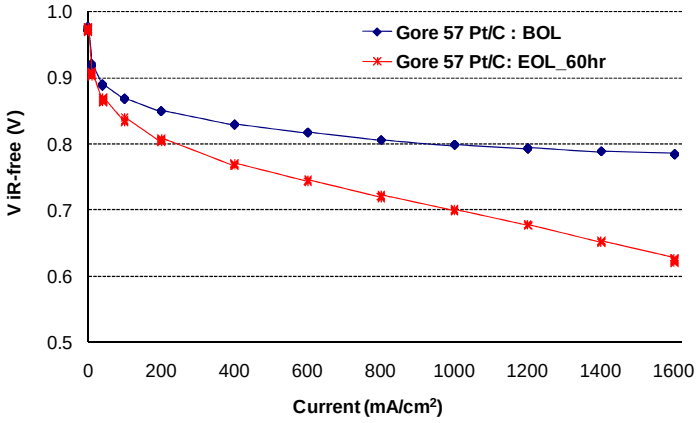


(b)

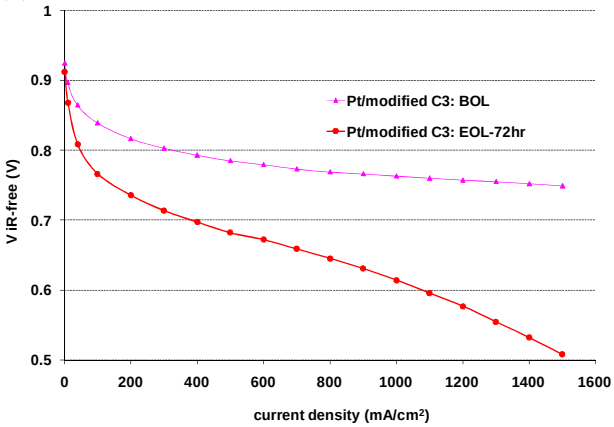


(c)

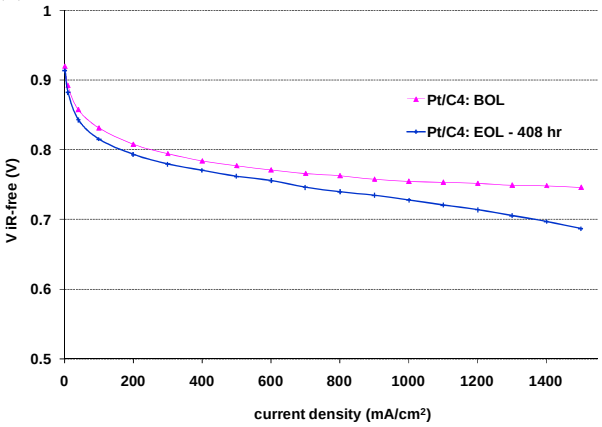


**Figure 9.** iR-free performance curves at BOL and EOL for (a) Gore 5710 Pt/C (b) 30% Pt/modified C3 and (c) 30% Pt/C MEA's after the 1.2 V potential hold tests in $H_2/O_2$, 100% RH at 80°C .

**Table 10.** Summary of the ECA, % Carbon loss, MEA resistance and $O_2$ performance loss at 1 A/cm$^2$ for the 30% Pt/C4, 30% Pt/modified C3 and a standard Gore 5710 Pt/C.

| Sample | Time after 1.2 V hold | ECA ($m^2$/g-Pt) | Total Cathode % Carbon loss | MEA Resistance (mΩ• $cm^2$) | $O_2$ performance (iR-free V) loss @ 1 A/$cm^2$ at EOL (mV) |
|---|---|---|---|---|---|
| Gore 57 Pt/C | BOL | --- | --- | --- | --- |
| | EOL- 1 hold for 60 h | --- | --- | --- | 98 |
| Pt/modified C3 | BOL | 31 | --- | 95 | 0 |
| | EOL – 3x24h = 72 h | 18 | 11.9 | 240 | 145 |
| Pt/C4 | BOL | 28 | --- | 79 | 0 |
| | EOL – 17x24h = 408 h | 19.2 | 26.7 | 187 | 27 |

The three Pt/C's were also subjected to an accelerated potential cycling protocol between 0.4 and 0.95 V [square wave 10s:10s] for 30,000 cycles. Although all the catalysts showed activity loss, the Pt/C4 MEA showed the lowest performance loss at high current density during the potential cycling with a cell voltage loss of only 49 mV at 1 A/cm$^2$ at the end of 30,000 cycles. Overall, the 30% Pt supported

catalysts on the C4 carbon showed better durability than either the standard Gore 57 Pt/C or the 30% Pt on modified C3 under both 1.2 V potential hold test and the accelerated potential cycling protocol and was down-selected for further incorporation and demonstration in a subscale fuel cell.

**2011:**

In FY2011, our efforts were focused towards optimization of the cathode catalyst layer in an MEA with 30% $Pt_2IrCr$ alloy catalyst to produce an optimum cathode catalyst layer capable of achieving good fuel cell performance in wide range of current densities.

Figure 10 shows the fuel cell performance curves in $H_2$/Air at different stages of the optimization process for the 30% $Pt_2IrCr$/C MEA in a full size (410 $cm^2$) WTP fuel cell compared to a baseline JMFC Pt/C MEA. The initial mass activity obtained for the alloy catalyst in the optimized MEA were 0.14 $A/mg_{PGM}$ compared to a mass activity of 0.19 A/mg PGM observed for the JMFC Pt/C MEA. This low activity is attributed to the low utilization of the catalyst in the MEA as seen by the low ECA of ~30 $m^2/g$ (vs. liquid cell ECA of 45 $m^2/g$ from RDE). However, clear evidence of improvement for high current density performance on $H_2$/Air in a WTP fuel cell is observed from these catalyst layer optimization steps. Our results show that lower catalyst loading of 0.3 $mg_{PGM}/cm^2$ in MEA can achieve high initial performances, although lower than the pure Pt/C. Extensive investigation into MEA fabrication process suggests that specific ink formulations significantly increase either mass transport properties or kinetic performance of alloy catalysts. This increase is attributed to the concentration of the ionomer in the ink formulations which results in the leaching of the Cr atoms from the catalyst surface to different concentrations and concurrently affects the kinetic and high current density performance in an MEA.

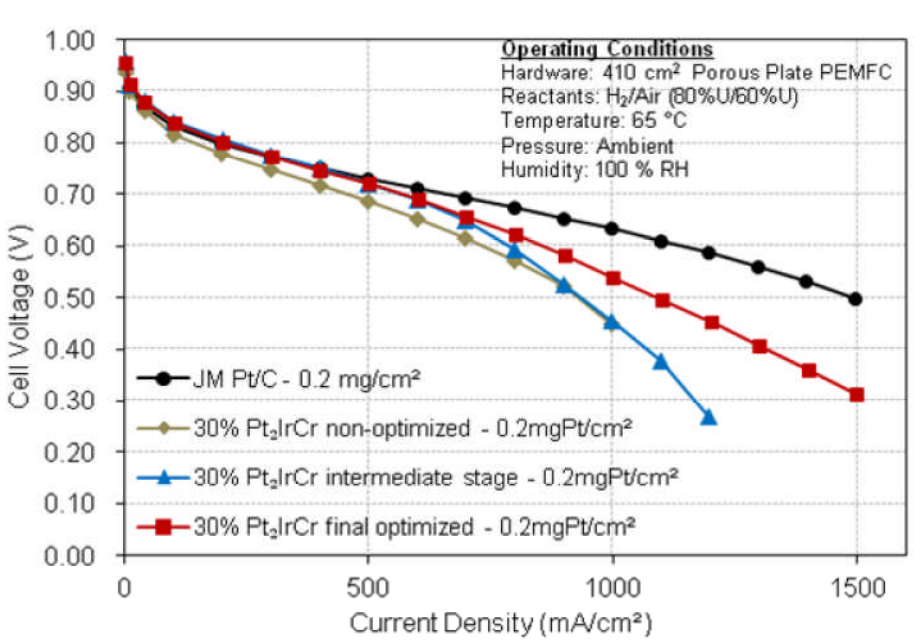


**Figure 10.** Fuel cell polarization curves in H2/air at 65°C in a water transport plate (WTP) fuel cell at 100% relative humidity (RH) and ambient pressure for an optimized, intermediate stage and unoptimized 30% $Pt_2IrCr$/C ternary alloy catalyst MEA compared to JMFC Pt/C (0.2mgPt/$cm_2$) MEA.

Figure 11 shows the (a) MA loss and (b) cell voltage at 0.8A/$cm^2$ on $H_2$/air for the 30% $Pt_2IrCr$/C and the JMFC Pt/C in a WTP fuel cell under two durability protocols. A higher rate of MA and performance loss is observed for the Pt-alloy compared to the pure Pt at both operating temperatures. This higher rate is

attributed to the lower stability of the transition metal in the Pt-alloy which results in the higher rate of MA loss. Additionally, any Cr leaching into the MEA would result in higher iR losses as observed by the cell voltage drop in the high current density region during cycling. Higher MA and cell voltage loss are observed with increase in operating temperature of the fuel cell for both Pt and Pt-alloy. This observation suggests that the rate of degradation of the catalyst is highly dependent on the operating temperature of the fuel cell and the cycling protocol. Due to insufficient data available in the literature on the durability of alloy catalysts under real life conditions, a short stack containing the Pt-alloy was built and its durability under an accelerated vehicle drive cycle protocol was evaluated.

(a)

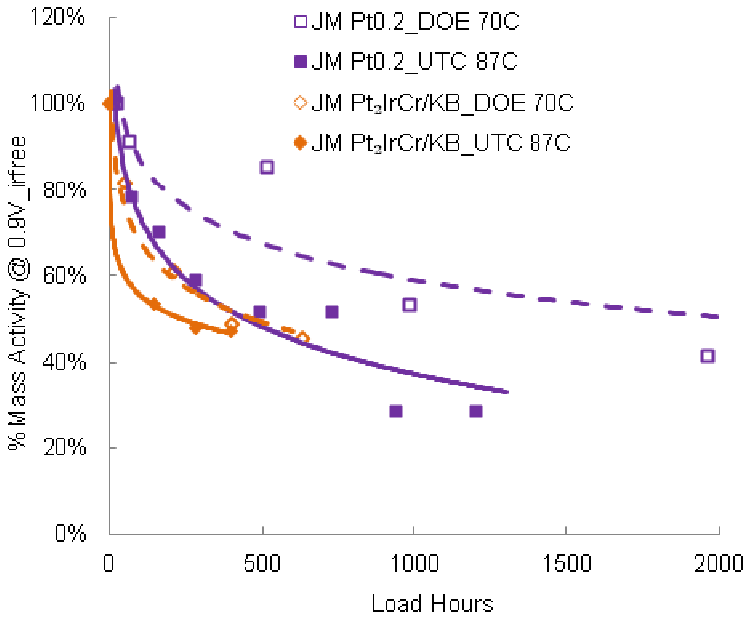


(b)

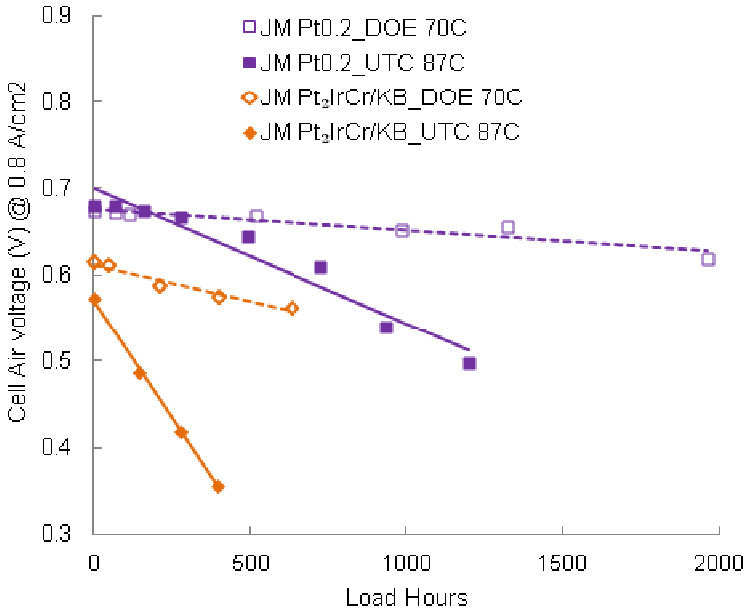


**Figure 11.** (a) Percentage mass activity and (b) cell air voltage at 0.8 A/cm$^2$ for the optimized 30% $Pt_2IrCr$/C MEA and JMFC Pt (0.2 mgPt/cm$^2$) MEA in a full-size WTP cell under two durability

protocols at 70°C and 87°C, respectively.

**Durable Carbon Support**

In FY2011, a scaled-up batch (200 g) of 20% $Pt_2IrCr$ on the down-selected stable carbon (C4) was prepared at JMFC and optimized for performance in sub-scale size (25$cm^2$) WTP cells. The effect of cathode catalyst layer compositions including ionomer EW and ratio of ionomer to carbon were extensively investigated using subscale fuel cell testing. Figure 12a shows performance curves for a preliminary optimized MEA compared to a commercial Gore 57 Pt/C in subscale size WTP fuel cells operating at 80 °C, 100% RH, 0 kPa backpressure. The Pt-alloy/C4 performance at high current operations is poor mainly due to the low surface area and poor mass transport properties of the carbon support C4. Figure 12b shows the iR-free cell voltages at various current densities (0.1, 1 and 1.5 A/$cm^2$) for a 0.2 $mg_{Pt}/cm^2$ 30% Pt/C4 and 20%$Pt_2IrCr$/C4 compared to a 30% Pt/C MEA obtained from a 25$cm^2$ WTP fuel cell testing at 80°C, 100% RH under $H_2/O_2$ at zero backpressure. Although the beginning of life performance for the Pt and Pt-alloy supported on C4 showed lower performance than that of the Pt/C, its performance after the 1.2 V potential hold tests showed considerable differences. After the fuel cell corrosion test of a total of 17 potential holds of 24 h each (408 h total) at 1.2 V, the 30% Pt/C4 and 20% $Pt_2IrCr$/C4 showed 59 mV and 92 mV loss respectively, at 1.5 A/$cm^2$ under $H_2/O_2$. While the alloy on C4 did not meet the 2010 DOE target of less than 30 mV iR-free $O_2$ performance loss at 1.5 A/$cm^2$ after 400h, the voltage loss after 360 h (15 potential holds of 24 h each) at 1.2 V for the alloy catalyst was only 40 mV.

(a)

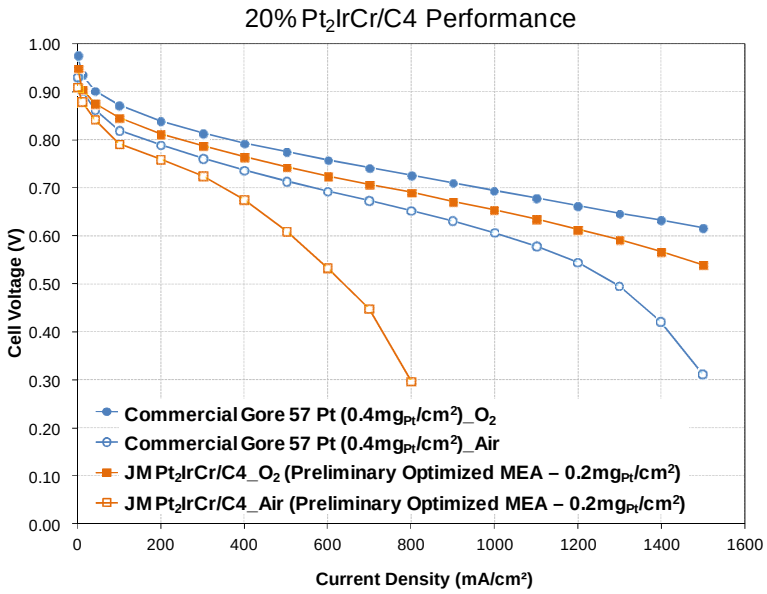


(b)

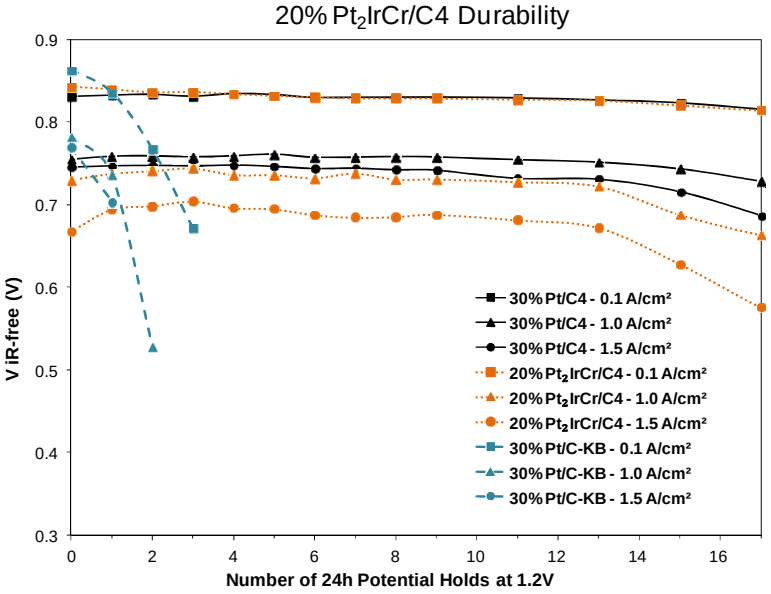


**Figure 12.** (a) Fuel cell performance curves at beginning of life for a 20% $Pt_2IrCr/C4$ compared to a standard 0.4 mgPt/cm$^2$ Gore 57 Pt/C MEA obtained from WTP subscale fuel cell (25 cm$^2$) testing at 80°C, 100% RH under $H_2$/air at zero backpressure and (b) $H^2/O^2$ performance at 0.1, 1 and 1.5 A/cm$^2$ after 1.2 V potential holds in $H_2/N_2$ at 80°C, 100% RH in subscale WTP cells for (0.2 $mg_{Pt}/cm^2$ loading) 30% Pt/C4 and 20% $Pt_2IrCr/C4$ compared to a 30% Pt/C MEA.

MEA optimization steps were performed for the 20% $Pt_2IrCr/C4$ to improve their performance in a subscale and full-size WTP fuel cell. Figure 13 shows the performance in $H_2$/Air for the 20% $Pt_2IrCr/C4$ in a full-size WTP cell at 65C after optimizing the MEA for suitable solvents and fabrication methods. The performance curves for the 30% $Pt_2IrCr/C_{KB}$ and the JMFC Pt/C are also included in Figure 13 for comparison. The cathode Pt loading for the 20% $Pt_2IrCr/C4$ was 0.14 mg/cm$^2$ compared to 0.2mg/$cm_2$ for

the Pt alloy/$C_{KB}$ and the JMFC Pt/C. Based on these results, the Pt alloy/C4, although stable towards corrosion, was not expected to meet performance requirements necessary for stack operation.

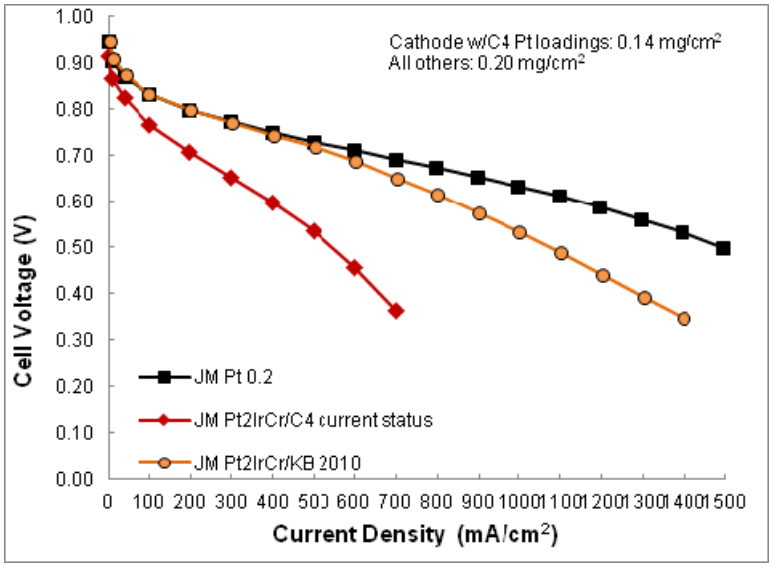


**Figure 13.** Polarization curves of $H_2$/Air performance for the preliminary optimized JM 10-129 (20% $Pt_2IrCr$/C4) MEAs compared to the optimized MEAs with JM10-112 (30% $Pt_2IrCr$/CKB) and JM Pt (0.2mg/$cm^2$) MEA in full size WTP cells.

**2012:**

In the final year, a significant amount of effort was focused towards optimization of the cathode catalyst layer in an MEA with 30% $Pt_2IrCr$ alloy catalyst to enable good performance at high current densities in a porous plate cell.

Figure 14 shows the sub-scale (25 $cm^2$) solid plate fuel cell performance curves in $H_2/O_2$and $H_2$/Air at 80 °C for the 30% $Pt_2IrCr$/C MEA with two different ionomer equivalent weights during the optimization process compared to a baseline Gore 5710 Pt/C MEA. The Performance at 100 mA/$cm^2$ is 0.87V for the electrode with 1000EW (cell 11-74) compared to 0.84V for the electrode with 1100EW (cell 11-67) for a loading of 0.3$mg_{PGM}$/$cm^2$.

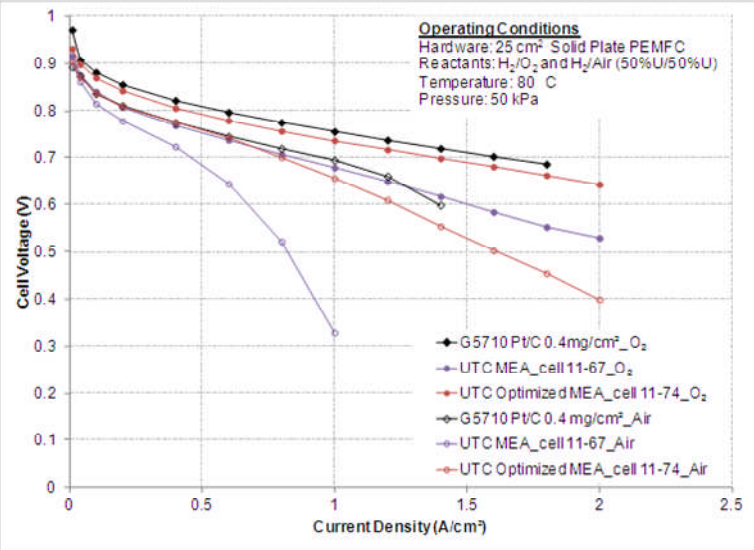


**Figure 14.** Polarization curves of $H_2/O_2$ and $H_2$/air performance for the preliminary optimization of JM 10-112 (30% $Pt_2IrCr$/CKB) MEAs compared to the Gore Pt (0.4mg/cm$^2$) MEA in sub-scale solid plate cells at 80°C, 50 kPa backpressure operation

Figures 15a and 15b shows the performance in $H_2/O_2$ and $H_2$/Air, respectively, for the (30% $Pt_2IrCr/C_{KB}$) in a porous plate cell at 65°C using various equivalent weight Nafion ionomer solutions in the cathode catalyst layer after optimizing the MEA for suitable solvents, ionomer/carbon (I/C) ratio and fabrication methods. The performance curves for a baseline JM Pt/C and the 2010 JMFC optimized 30% $Pt_2IrCr/C_{KB}$ MEA is also included for comparison. Table 11 summarizes the performance of all the MEAs. As shown in figure 15, the MEAs using different ionomer solutions in the catalyst layer of the cathode electrode results in higher performance than the 2010 JMFC optimized MEA in both oxygen and air at low current density regions. Moreover, the electrode with 1000EW shows significant improvement in the mass activity (0.17A/mg$_{PGM}$) and the corresponding $H_2$/air performance for the 2011 UTC optimized MEA shows a 53 mV improvement at 1A/cm$^2$ compared to the 2010 JMFC optimized MEA. This improvement in activity and performance is primarily due to the better utilization of the catalyst and improved mass transport resistance in the MEA.

(a)

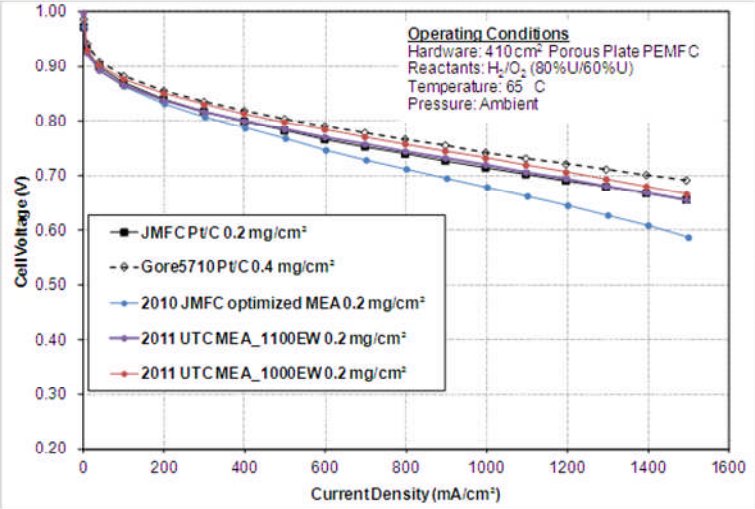


(b)

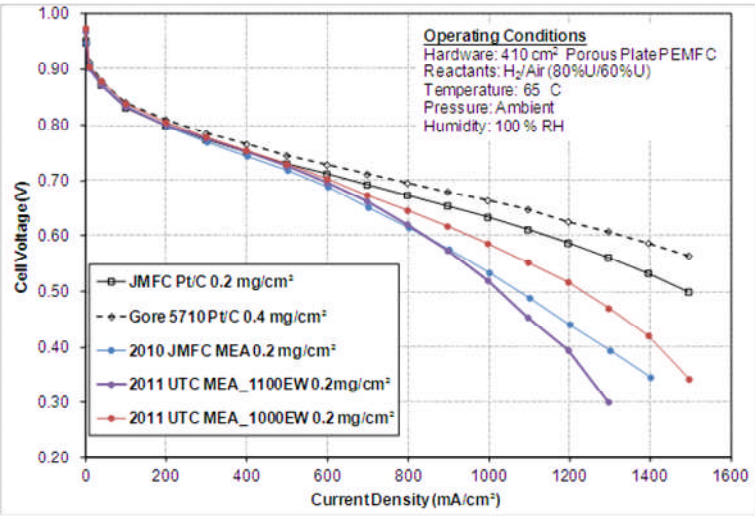


**Figure 15.** Polarization curves of (a) $H_2/O_2$ and (b)$H_2$/air performance for the optimization of JM 10-112 (30% $Pt_2IrCr/C_{KB}$) MEAs compared to JMFC Pt (0.2 mg/cm$^2$) MEA in full-size porous plate cells at 65°C, 0 kPa backpressure operation.

Table 11. Summary of $H_2/O_2$ and $H_2$/air performance of the 30% $Pt_2IrCr/C$ alloy catalyst MEAs compared to a commercial Gore Pt/C (0.4 $mg_{PGM}/cm^2$) and JMFC Pt/C (0.2 $mg_{PGM}/cm^2$) MEA.

| Cell | Voltage at 0.1A/$cm^2$ in $H_2/O_2$ (V) | Voltage at 1A/$cm^2$ in $H_2$/Air (V) | iR at 1A/$cm^2$ in $H_2$/Air (V) |
|---|---|---|---|
| JM Pt/C (0.2) | 0.871 | 0.634 | 0.079 |
| Gore5710 Pt /C(0.4) | 0.883 | 0.664 | 0.062 |
| JMFC MEA | 0.864 | 0.533 | 0.093 |
| UTC MEA 1100EW | 0.866 | 0.520 | 0.076 |
| UTC MEA 1000EW | 0.886 | 0.586 | 0.084 |

20-cell Stack Validation

In FY2011, a 20-cell short stack built at UTC containing the 30%$Pt_2IrCr/C_{KB}$ MEAs completed 2000 hours of cycling using the accelerated lifetime test (ALT) conditions developed under a DOE funded project at UTC Power titled "Improved Accelerated Stress Tests Based on Fuel Cell Vehicle Data" (contract number: DE-EE0000468). The short stack contained four Pt MEAs as references and sixteen alloy catalyst 30%$Pt_2IrCr/C_{KB}$ MEAs. All MEAs were manufactured by JMFC with a cathode Pt loading of 0.2 $mg_{PGM}/cm^2$ and anode Pt loading of 0.1 $mg_{PGM}/cm^2$. After conditioning, BOL performance was tested in both oxygen and air. Cell resistance was measured by the $H_2$-pump method.

The average performance of the cells in $O_2$ and air with the alloy catalyst was lower than the Pt catalyst cells as shown in Figure 16. The resistance of 79±5 $m\Omega.cm^2$ in the alloy catalyst cells was similar to that of Pt catalyst cells (73±3 $m\Omega.cm^2$). In general, the Pt catalyst outperformed the alloy catalyst by 100 mV in air at 1 $A/cm^2$. This performance gap is ascribed to oxygen permeability and proton concentration losses in the cathode due to Cr ion contamination in the 30%$Pt_2IrCr/C_{KB}$ MEA.

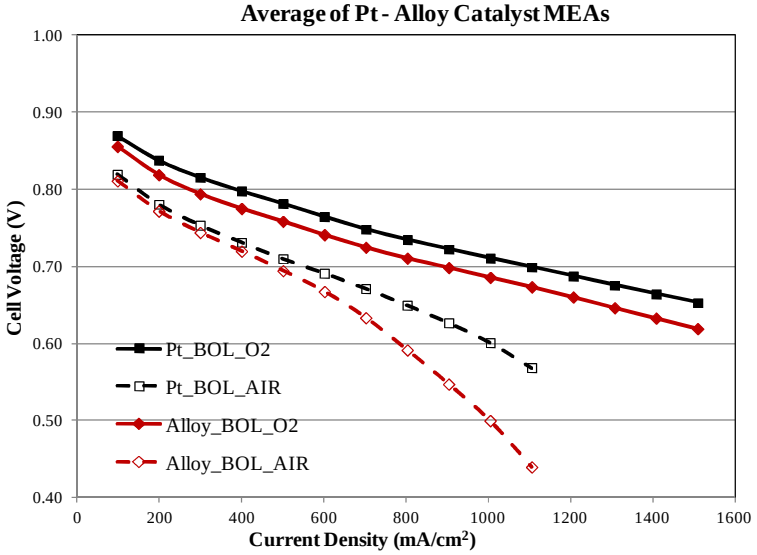


Figure 16. BOL performance of Pt/C and the alloy catalyst (30% $Pt_2IrCr/C_{KB}$) in the 20-cell stack

Figure 17a shows the average voltage at 800 mA/cm$^2$ in air for both Pt/C and the alloy catalysts decrease with load cycles at an average voltage decay rate of 20 μV/h and 19 μV/h (or μV/cycle) respectively. Previously, a higher rate of activity and performance loss was observed for the Pt-alloy compared to the pure Pt under a load cycling test in the full-scale water transport plate (WTP) cells (85 μV/h compared to 36 μV/h). In terms of the catalyst activity, no current density steps lower than 100 mA/cm$^2$ were measured during the polarization curve measurement and hence mass activity cannot be determined from the 20-cell stack data. Although from the BOL oxygen curves in Figure 16, the Pt/C cells show slightly higher average voltage than the alloy catalyst cells at 100 mA/cm$^2$, during the load cycling, the alloy catalyst shows a higher performance compared to the Pt/C at a lower current density of 16 mA/cm$^2$(figure 17b). After periodic diagnostic tests, both Pt and Pt alloys show partial performance recovery. This was mostly due to the removal of Pt oxides on catalyst surfaces at high current density. During subsequent load cycles following the diagnostic tests, it's noticeable that the alloy catalyst had initial lower voltage or activity decay than Pt/C, which was mostly due to the slower surface Pt oxidation. However, with continued load cycling, the alloy performance decreases slowly while the Pt/C catalyst quickly reaches a steady state voltage. This difference is attributed to alloy catalyst compositional changes with the loss of Cr as discussed below.

(a)

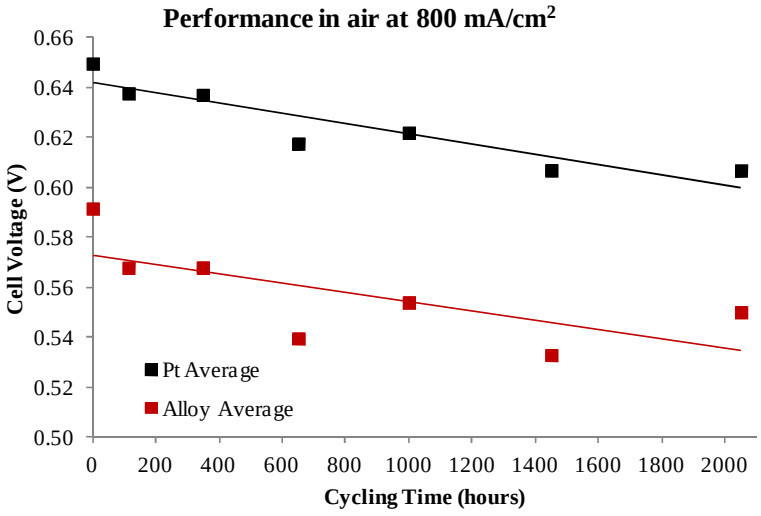


(b)

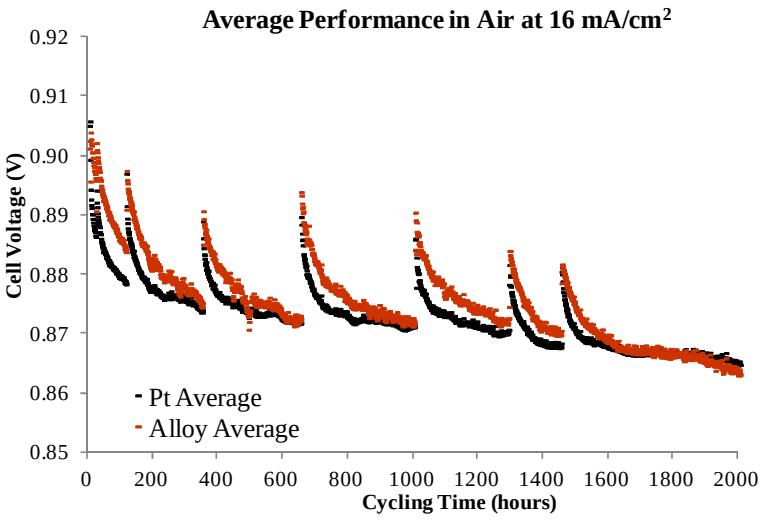

Figure 17. 20-cell short-stack performance decay during load cycles for Pt/C and the alloy catalyst (30% $Pt_2IrCr/C_{KB}$) in air at (a) 800 mA/cm$^2$ and (b) 16 mA/cm$^2$

Post-test observations including catalyst composition and electrode structure were conducted on the degraded MEAs after the stack tear down. Figure 18 shows the presence of Pt, Ir, and Cr in the MEA as measured by electron micro probe analysis (EMPA) from one of the cells from the 20-cell stack after 2000 hours of cycling. The EMPA image shows a significant amount of Cr in the membrane and the anode electrode after durability cycling.

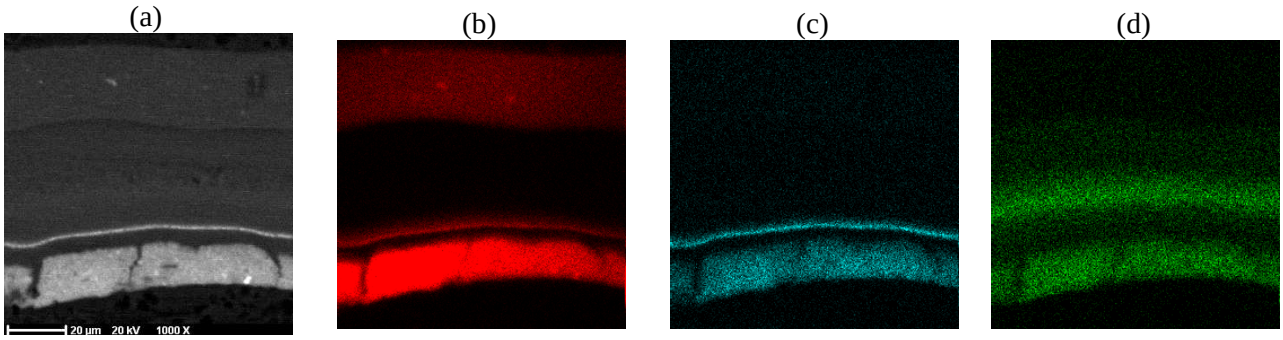


**Figure 18.** EMPA elemental map in the MEA after 2000 hours of accelerated cycling in a 20-cell stack.

Table 12 shows the ratio of Pt, Ir and Cr in the cathode electrode before and after cycling as determined by Energy Dispersive Spectroscopy (EDS). A significant reduction (~50%) in Cr concentration in the electrode is comparable to the EMPA elemental analysis shown in figure 18. TEM image analysis of the cathode catalyst particles did not show significant increase in particle size for the alloy catalyst before (5nm) and after cycling (5.6 nm). However, a pure Pt catalyst from a baseline MEA with Pt/C in the cathode electrode showed a significant increase in particle size before (~2nm) and after (5.6nm) cycling for 2000 hours in the 20-cell stack. Based on the post-test analysis shown above, it is concluded that the primary durability loss in the 30% $Pt_2IrCr/C$ alloy catalyst is due to the transition metal dissolution (~50% loss) from the alloy catalyst.

**Table 12.** Ratio of Pt, Ir and Cr in the cathode electrode before and after durability cycling in the 20-cell stack as determined by Energy Dispersive Spectroscopy (EDS)

| 30% $Pt_2IrCr$ alloy composition | Pt | Ir | Cr |
|---|---|---|---|
| Initial wt.% | 61.4 | 30.4 | 8.2 |
| Initial atomic ratio | 1.0 | 0.50 | 0.50 |
| Final wt.% | 71.0 | 24.2 | 4.8 |
| Final atomic ratio | 1.0 | 0.35 | 0.25 |

## Core-Shell Pt Catalysts

### 2008:

Zhang et al. showed the feasibility of Pt ML deposition on mixed PGM and transition metal cores to reduce the usage of Pt for the oxidation reduction reaction [6]. Modeling the impact of different cores and Pt ML shells is being carried out under this project at TAMU. This work is also being complemented with synthesis of core-shell structures. Pt ML on Ir and $Pd_3Co$ cores were synthesized and evaluated for durability and electrochemical activity using the RDE technique. Ir cores were synthesized at UTCP and sent to BNL for Pt ML deposition. The existing oxides on the Ir cores were first reduced by annealing at 500°C in a $H_2$ environment prior to the Pt deposition. The carbon-supported Ir and $Pd_3Co$ cores were mixed with a Nafion® solution and deposited onto an RDE electrode as a film. Onto this film, a Pt ML was deposited by displacing Cu that was pre-deposited via the Cu under potential deposition (UPD) method.

The mass activity data measured using the RDE technique for the two cores mentioned above are shown in Figure 19. The mass activity is presented normalized to the Pt and on the electrodes. The mass activity of the Pt baseline (TEC10E50E-HT, 50% TKK catalyst) is approximately 0.18 A/mg.

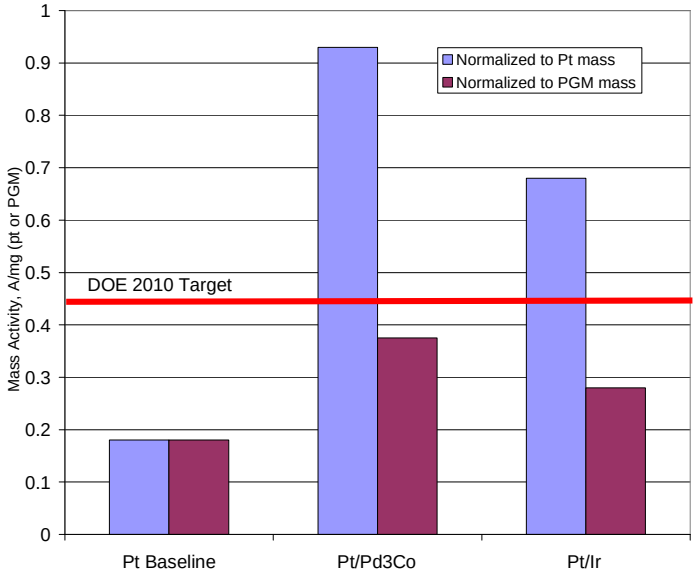


**Figure 19.** Mass Activities of 1 $Pt_{ML}$ on $Pd_3Co$ and Ir Cores

The mass activity for the ML catalysts achieved in FY2008 approached the DOE 2010 target of 0.44 $A/mg_{PGM}$ (0.37 and 0.28 $A/mg_{PGM}$ for the $Pd_3Co$ and Ir cases, respectively, shown in Figure 19).

### 2009:

The primary focus of core-shell development in FY2009 was (a) to synthesize Pt ML catalysts on $Pd_3Co$ and Ir cores using scalable chemistries without compromising the intrinsic activity of the catalyst as demonstrated by BNL and (b) to characterize the structure of the core-shell catalysts. For this purpose, a large batch (30 g) of $Pd_3Co$ and Ir cores were synthesized at JMFC. Subsequently, a large 5g batch Pt ML core-shell catalyst was synthesized successfully by JMFC via a chemical method. A 300 mg batch of Pt ML core-shell catalyst was also prepared by BNL using the galvanic displacement of underpotentially deposited (UPD) Cu ML. High mass activities of >1 A/mg Pt are observed for a Pt ML on a carbon supported $Pd_3Co$ nanoparticle on a glassy carbon tip under RDE test conditions. However, correcting for the PGM in the core, the activity normalized to total PGM content is reduced. Figure 20 shows the mass activity based on PGM loading for three $Pt_{ML}/Pd_3Co$ core-shell catalysts (i) prepared via Cu UPD on an

RDE tip (red) (ii) 300 mg batch prepared using Cu UPD (dark blue) and (iii) large scale (5g) batch prepared via chemical methods (light blue) compared to a commercial TKK 50 wt% Pt/C (black). The $Pt_{ML}/Pd_3Co/C$ prepared via Cu UPD intermediate show mass activities ~1.5 times higher than the standard Pt/C. However, the large scale Pt core-shell catalyst synthesized via chemical method shows little enhancement on a total PGM basis.

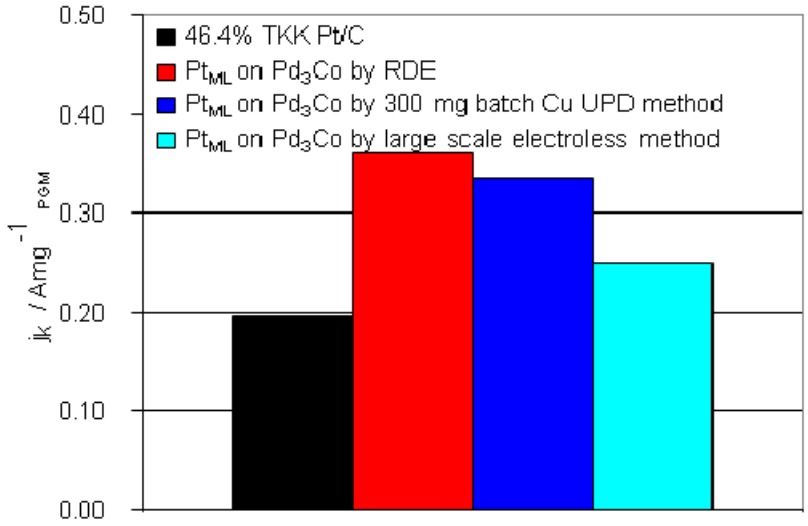


**Figure 20.** PGM mass activity vs. RHE for a commercial Pt/C catalysts and a PtML on $Pd_3Co/C$ catalysts synthesized via different methods obtained from RDE testing in 0.1 M $HClO_4$ at 1,600 rpm, and 10 mV/s. The same batch of $Pd_3Co/C$ was used for all Pt ML core-shell catalysts.

In situ extended x-ray absorption fine structure studies show that the surface oxidation on $Pt_{ML}/Pd_3Co$ prepared by electroless method is very similar to that of Pt/C. A STEM study indicates that the as-prepared $Pt_{ML}/Pd_3Co$ sample has a broad size distribution, from 3-10 nm. HAADF-STEM profile combined with Pd EELS signal for individual nanoparticles within the catalyst structure provides compelling evidence for the presence of Pt shells around the Pd containing cores with thickness varying from 0.4-1 nm. Figure 21a shows a representative TEM image obtained for a ~7 nm $Pt_{ML}/Pd_3Co/C$ nanoparticle synthesized using Cu UPD methods and the corresponding HAADF-STEM – EELS profile showing a 0.5-0.6 nm thick Pt shell on a Pd containing core of ~ 5.5 nm (figure 21b). Similar structural properties are observed for Pt coatings applied to the same $Pd_3Co$ core using the scalable synthesis route. However, after 6,500 potential cycles between 0.7–1.1 V, these samples show a small particle growth and a similar size distribution compared to the as-prepared catalyst. The particle size change does not account for the total electrochemical surface area loss of the catalysts during cycling. This was found to be consistent with STEM observations which indicate a lower particle density and an uneven shell thickness for the post-cycling test in comparison to the as-prepared sample.

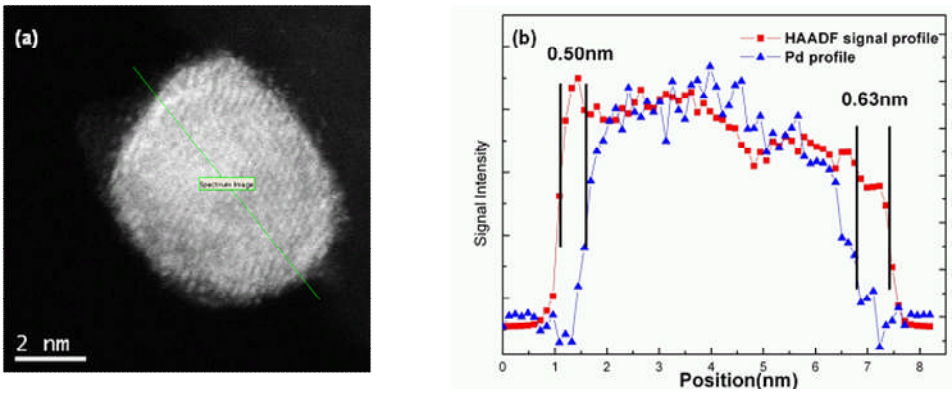


**Figure 21.** (a) High resolution STEM images of a PtML/$Pd_3Co$/C particle synthesized using Cu UPD method and (b) the corresponding cross-sectional compositional line profiles of HADDF-STEM (information of particle size) and Pd M-edge EELS signal (information of Pd distribution along the line) from image (a). The core-shell structure as well as the shell thickness can be directly derived from the difference between HADDF signal and EELS Pd signal.

**2010:**

The primary focus of core-shell development was (a) to synthesize Pt ML catalysts on Pd3Co and Ir cores using scalable chemistries without compromising the intrinsic activity of the catalyst as demonstrated by BNL and (b) to incorporate these advanced catalyst concepts in an MEA. Previously, a large batch (30 g) of Pd3Co and Ir cores and 5g batch Pt ML core-shell catalyst were synthesized successfully by JMFC via a chemical method.

Figure 22 shows the mass activity based on PGM loading for a scaled-up $Pt_{ML}/Pd_3Co$ core-shell catalyst prepared via chemical methods and a pure Pt/C catalyst obtained from RDE and MEA testing. Although the mass activity obtained on the pure Pt/C in an MEA is slightly lower than that obtained from RDE measurements, the $Pt_{ML}/Pd_3Co$ core-shell catalyst shows a significant lower activity in an MEA (0.044 A/mg PGM) than from RDE measurements (0.254 A/mg PGM). This is mainly attributed to (a) instability of $Pt_{ML}/Pd_3Co$ at 80ºC under MEA test conditions and (b) the incomplete or non-uniform coverage of Pt on the core $Pd_3Co$ particles. Detailed studies of the $Pt_{ML}/Pd_3Co$ core-shell catalysts in 1M $H_2SO_4$ solution at 80 °C using electrochemical and physical characterization using inductively coupled plasma (ICP) shows substantial loss of Co and Pd on exposure to the acid which indicated incomplete coverage of Pt.

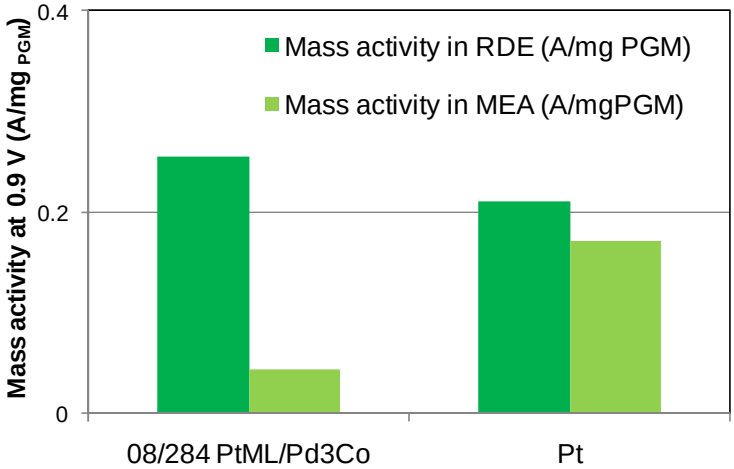


**Figure 22.** Comparison of PGM mass activity of $Pt_{ML}/Pd_3Co$ and a Pt/C obtained from RDE and MEA testing.

To investigate the effect of Pt deposition route on catalyst activity and stability a direct comparison was made between $Pt_{ML}/Pd_3Co$ prepared by the JMFC scaleable chemical route (catalyst 09/71) and a 2 g catalyst batch prepared by BNL using the electrochemical Pt deposition route (catalyst 10/12). While these materials had already been assessed and shown to be equivalent by ex-situ characterisation and in the RDE, investigation under MEA conditions was required. Equivalent mass activity, extrapolated to 0.14 A/mgPt at 900 mV, was observed for core shells prepared by both routes as shown in Figure 23(a). Although the sample prepared by the electrochemical Pt deposition shows a slower rate of ECA loss, equivalent and substantial Pd dissolution into the electrolyte in cycles to 1.0 V in 1M $H_2SO_4$, 80°C is observed in both catalysts (figure 23b), regardless of the Pt deposition route used. Lower Co loss from the core shell prepared at BNL using the electrochemical Pt deposition route (catalyst 10/12) is due to the lower initial Co content of the material; acid exposure during Pt electrochemical deposition at BNL removed Co leading to a $Pt_{ML}/Pd_8Co$ composition for catalyst 10/12.

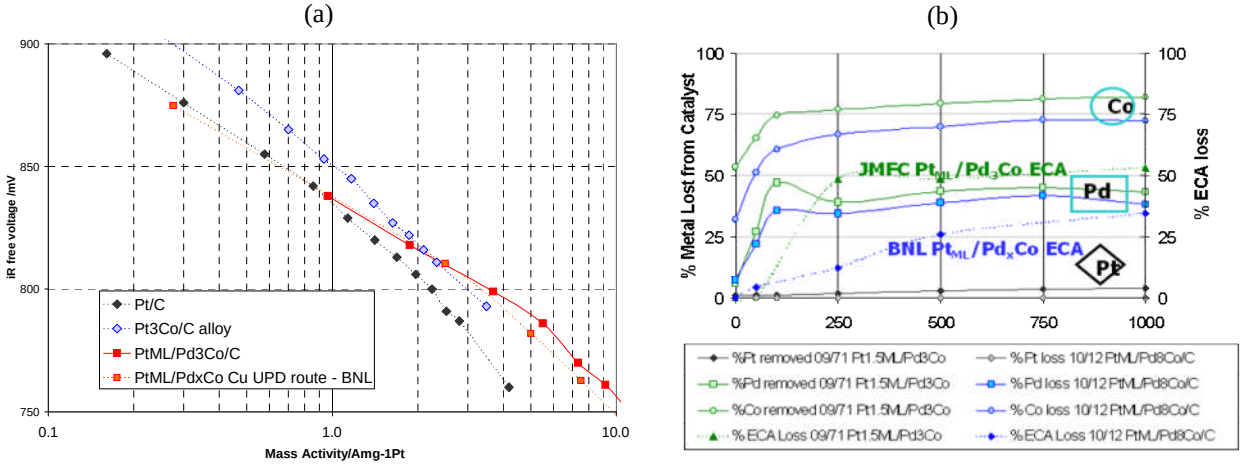


**Figure 23.** (a) iR correct oxygen mass activity, 150 $kPa_{abs}$, 80°C, $Pt_{ML}/Pd_3Co/C$ (catalyst 09/71 JM chemical route), $Pt_{ML}$/PdxCo/C Cu UPD route (catalyst 10/12 BNL electrochemical route) and Pt/C and $Pt_3Co/C$ references and (b) stability of $Pt_{ML}/Pd_xCo/C$ prepared by chemical and electrochemical routes in 1000 voltage cycles, 0.6-1.0V, 50 mV/s, 1M $H_2SO_4$, 80°C, shown as % ECA loss and % metal loss from catalyst into electrolyte.

Further analysis of $Pt_{ML}/Pd_8Co$ prepared at BNL under RDE type conditions, equivalent to those shown in Figure 23(b) for JMFC prepared $Pt_{ML}/Pd_3Co$, showed very comparable trends of minimal Pd dissolution. Thus equivalent good activity for JMFC and BNL prepared materials under RDE conditions and the lower activity under MEA, 80°C, and more acidic conditions may be rationalized in terms of Pd losses and hence integrity of the Pt monolayer under the different testing regimes. The segregation of Pd and X to the surface of various $Pt_{ML}/Pd_3X$ (X = Co, Fe, Cr etc) in the presence of adsorbed oxygen (at high potentials) is in agreement with modeling work by TAMU within this project. [17]

**2011:**

In 2011, BNL focused on a "cation-wash" procedure to improve the stability of core-shell nanoparticle catalysts which removes the non-noble components (as in PdCo, PtNi alloys) from the surface and sub-surface layers by exposing the alloy to a noble metal cation such as, $Pd^{2+}$, $Ir^{3+}$, $Pt^{2+}$ which displaces Co or Ni from the top surface layer and block further dissolution unlike the acid wash. This cation wash and the introduction of a noble metal interlayer resulted in a very active catalyst. However, their stability is still questionable based on the cyclic voltammetry which indicated the formation of a sub-surface H, which may decrease the stability. Annealing the samples to improve the stability did not provide a clear benefit.

The activity and stability of the $Pt_{ML}$/Ir core shell system was also explored. 3-4 nm Ir cores were prepared on Ketjen EC 300J and characterised ex-situ and by cyclic voltammetry and electrochemical cycles. Mass activity of 0.3 A/mgPt (extrapolated) at 900 mV on oxygen in MEAs was also observed for $Pt_{ML}$/Ir, although once Ir cost is included no benefit is present over Pt only (0.2 A/mgPGM assuming Ir cost remains ~ 25% that of Pt). Durability of $Pt_{ML}$/Ir in MEAs was measured using 0.7-0.9 V iR free $H_2$/Air cycling over 40,000 cycles and showed similar decay behavior to the Pt reference. Significantly higher stability to electrochemical cycles was observed for Ir cores compared to $Pd_3X$, and this translated through to the Pt coated versions. Figure 24 illustrates the substantially lower Ir dissolution from the $Pt_{ML}$/Ir system compared to $Pt_{ML}/Pd_3Co$ during cycles from 0.6-1.0 V, 50 mV/s, 1M $H_2SO_4$, 80°C.

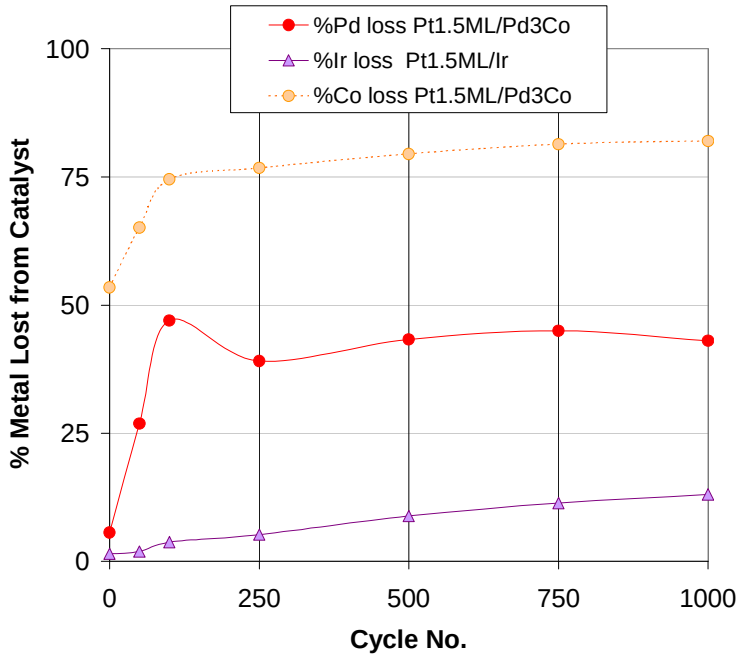


**Figure 24.** Stability comparison of $Pt_{1.5ML}$/Ir/C with $Pt_{ML}/Pd_3Co$/C in 1000 voltage cycles, 0.6-1.0 V, 50 mV/s, 1M $H_2SO_4$, 80°C, shown as % ECA loss and % metal loss from catalyst into electrolyte.

Figure 25a shows a comparison of Pd dissolution from a $Pt_{1.5ML}/Pd_3Co$ catalyst (09/71) under different potential cycling regimes. Even in the absence of potential cycling during a potential hold at 0.9 V at 80°C in 1M $H_2SO_4$, substantial loss in Pd loss is observed (shown in Figure 25a); either as consequence of pinholes in the Pt shell or rearrangement of the surface under oxidizing conditions. Significant Pd loss and loss of the uniform Pt overlayer may explain the lower activity observed in MEAs for these systems compared to RDE as shown in Figure 25b for selected core-shell catalysts. While $Pt_{ML}$/Ir intrinsic activity under RDE conditions is lower than $Pt_{ML}/Pd_3Co$, the higher stability of Ir cores compared to $Pd_3X$ in the MEA environment results in improved MEA performance for $Pt_{ML}$/Ir.

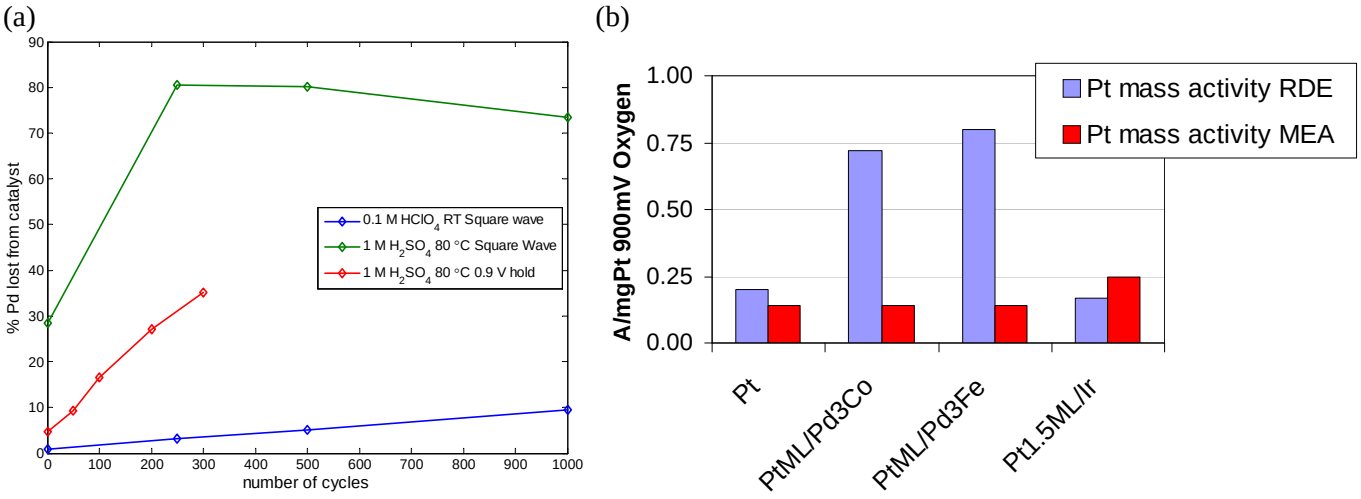


**Figure 25.** (a) % Pd dissolution from $Pt_{1.5ML}/Pd_3Co$ coreshell under different regimes, including 0.9V hold performed for equivalent time to cycles in cycling protocols, and (b) Mass activity gap between RDE and MEA for $Pt_{1.5ML}/Pd_3Co$ compared to $Pt_{ML}/Ir$ core shell systems.

As mentioned earlier, studies were also conducted to investigate the effect of the "cation wash" using noble metal salts to improve the stability of core-shell nanoparticle catalysts as recommended by BNL. The application of the Pd and Ir ion wash steps to the $Pd_3X$ cores were pursued to exchange surface base metal atoms with Pd or Ir as shown schematically in Figure 26

(a)

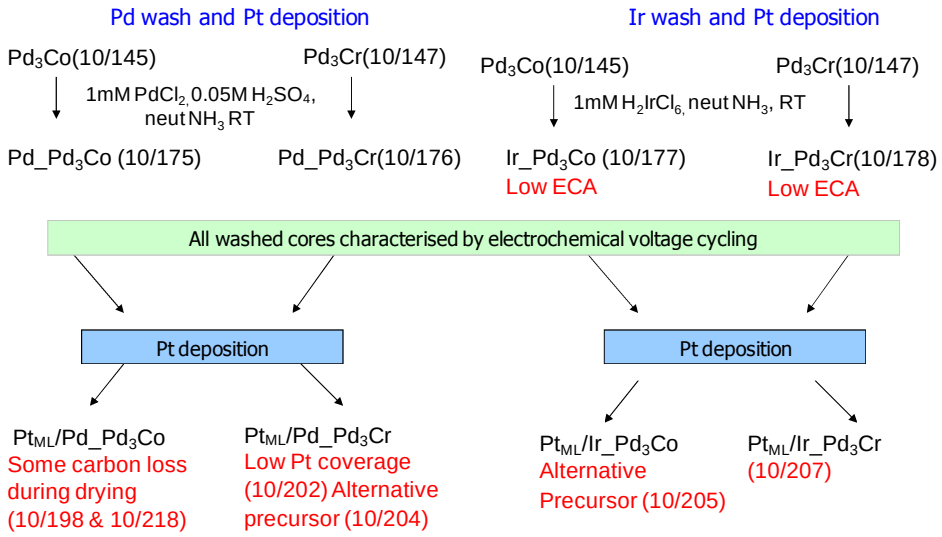


**Figure 26.** Schematic showing Pd and Ir ion wash treatments and subsequent Pt deposition.

Cross comparing results from ICP, XRD and ECA measurements, Pd washed $Pd_3Co$ and $Pd_3Cr$ cores show little difference from the non-washed core materials and unexpectedly low initial ECAs were observed for the Ir ion washed $Pd_3Co$ and $Pd_3Cr$ samples. Potential cycling measurements between 0.6-1.0 V in 1 M $H_2SO_4$ at 80 °C also showed very similar trends in ECA loss between washed and as

prepared cores. Moreover, $Pt_{ML}$ deposition on Pd and Ir cation washed $Pd_3Cr$ cores resulted in inclomplete Pt coverage of 0.65 ML similar to non-washed $Pd_3Cr$ sample. However, an alternate precursor for the deposition of $Pt_{ML}$ resulted in a complete Pt coverage of the $Pd_3Cr$ cores (JM 10/204).
Preliminary MEA activity data of JM 10/204 ($Pt_{ML}$ on a Pd washed $Pd_3Cr$ core using an alternative Pt precursor) and JM 10/198 ($Pt_{ML}$ on the Pd washed $Pd_3Co$ core) are shown in Figure 27. Both these core shell materials show lower activity than previously tested samples. In the case of JM 10/198 ($Pt_{ML}$ on the Pd washed $Pd_3Co$ core), the low mass activity is a result of sintering that was observed during the catalyst synthesis. Moreover, JM 10/204 ($Pt_{ML}$ on a Pd washed $Pd_3Cr$ core using an alternative Pt precursor) showed no benefit from the new Pt precursor.

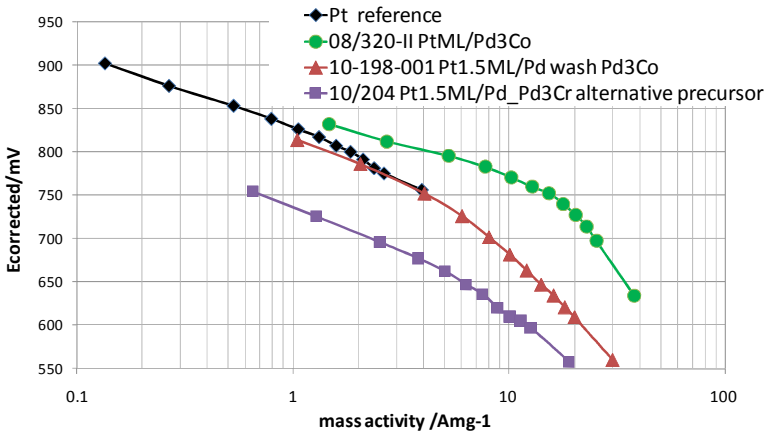


**Figure 27.** Mass activity in MEAs of $Pt_{ML}/Pd_3Co$ (JM 08/320), $Pt_{1.5ML}$/Pd washed $Pd_3Co$ (JM 10/198) and $Pt_{1.5ML}$/Pd washed $Pd_3Cr$ (JM 10/204) core shell catalysts in a solid plate fuel cell at 80 °C.

The "cation wash" using noble metal salts to improve the stability of core-shell nanoparticle catalysts as recommended by BNL was designed to exchange base metal atoms on the surface of $Pd_3X$ cores with either Pd or Ir, reducing dissolution of core elements and improving uniformity of the Pt overlayer in the final core shell. As previous attempts to deposit Pt onto $Pd_3Cr$ cores had resulted in incomplete Pt coverages, the ion wash treatment was also explored for the $Pd_3Cr$ system in addition to the $Pd_3Co$ cores. Overall, four types of material were generated, $Pt_{ML}$/Pd wash/$Pd_3Co$, $Pt_{ML}$/Ir wash/$Pd_3Co$, $Pt_{ML}$/Pd wash/$Pd_3Cr$ and $Pt_{ML}$/Ir wash/$Pd_3Cr$. Further, an alternative Pt precursor was also explored in some instances. Electrochemical stability measurements for these catalysts were performed under 0.6-1.0 V, 50 mV/s, 1M $H_2SO_4$, 80°C conditions and the Pd and Co/Cr dissolution were evaluated similar to the method described above. A 25% loss in Pd after only 50 cycles was observed for the cation-washed catalysts and hence no significant improvement in stability was observed under these conditions compared to the non-ion washed versions. Furthermore, catalyst $Pt_{ML}$/Pd wash/$Pd_3Co$ also showed a loss in carbon during the catalyst synthesis process resulting in a sintered product with lower carbon content and higher metal assays. MEA performance measurements on selected samples showed lower or equivalent activities compared to previously prepared samples without a Pd/Ir ion wash step. Moreover, incorporation of the Pd or Ir ion wash step was also not beneficial in improving Pt deposition with the $Pd_3Cr$ core system and coverage of only 0.65ML was achieved. In light of the results presented here, Pd losses from the $Pt_{ML}/Pd_3X$ systems in the 1M $H_2SO_4$, 80°C conditions (analogous to the MEA operating environment) could not be mitigated by the ion wash process.

In summary, application of various procedures to the $Pt_{ML}/Pd_3Co$ system such as improved reduction, acid leaching or Pd/Ir ion wash treatment of the precursor cores prior to Pt coating did not improve either MEA performance or reduce Pd and Co/Cr dissolution. Thus, the high activity of this novel catalyst type, as indicated by RDE results was not observed in MEAs. Although improved stability and acceptable

performance in MEAs were observed for $Pt_{ML}$/Ir core shell catalysts, no cost benefit is achieved over Pt only catalysts based on total PGM. Based on these results, a "**No-Go**" decision was made for this class of core-shell catalysts.

## CONCLUSIONS AND FUTURE DIRECTIONS

### Dispersed Pt Alloy Catalyst

Many factors such as structure, particle dispersion, particle size, type of carbon support used etc, influence the electro-catalytic activity of Pt and Pt alloy nanoparticles. Previously, within this project it was established that a 30 wt% Pt in $Pt_2IrCo$ exhibited an activity almost two times higher than 20 and 40 weight percent samples. In the past years, a significant amount of effort was focused towards development and optimization of the composition of PtIrM (M= Co, Cr, Ni, Fe etc.,) alloy catalysts to further improve electro-catalytic activity and enable lower PGM loading. This involved synthesis, physical characterization (using inductively coupled plasma, transmission electron microscopy and X-ray diffraction), electrochemical characterization in a liquid electrolyte using rotating disk electrode (RDE) and verification in an MEA. These catalysts were also subjected to potential cycling. The potential cycling was interrupted at various intervals during the experiment to measure the electrochemical surface area (ECA) and oxygen reduction reaction activity. Based on the activity and durability results obtained on a number of PtIrM/C catalysts, 30%$Pt_2IrCr$/C was down-selected for scale-up and verification in a multi-cell stack.

The effects of MEA compositions were studied for the scaled-up 30% $Pt_2IrCr$/C in full-size WTP fuel cells. The electrode optimization studies clearly show that MEA ink formulations and processing methods significantly impact the electrode structure in an MEA and their performance under high current density operations. Short stack containing the Pt-alloy was built and it's durability under an accelerated vehicle drive cycle protocol showed that the durability loss was primarily due to the transition metal dissolution (~50% loss) from the alloy catalyst. Although some progress was made to overcome key barriers for the incorporation of the 30% $Pt_2IrCr$ in an MEA such as low catalyst utilization in electrodes, the transition metal stability under operating conditions remains a concern.

Current UTC Power experience shows that alloy catalyst layers with low PGM loading exhibit increased mass-transport limitations, likely due to the surface properties of the alloys. The key challenge was to translate the potential performance offered by the alloy catalysts into a practical MEA structure, operating under real-life conditions. It is now recognized that a focus on MEA optimization during the early stages of catalyst development is essential to identify and understand the limits of alloy catalysts and their impact on the high current density performance.

### Durable Carbon Supports

In an effort to identify an alternate durable carbon support capable of withstanding high voltage spikes relevant for automotive applications, several carbon supports were evaluated by subjecting pellets of these carbon samples to a constant potential hold of 1.4 V in 0.5 M $H_2SO_4$ at 80 °C for 5 hours. Based on the weight loss after the 5 hour potential hold and also on the carbon loss as $CO_2$, two carbon supports were down-selected for further fuel cell testing. Several challenges still remain unanswered in this program partly due to the intrinsic properties of the carbon supports, which resulted in large particle size Pt and Pt-alloy catalysts with low mass activities due to poor utilization. This can be addressed via novel ways of catalyst synthesis methodologies and better control of synthesis process parameters. However, considerable effort is required to understand and identify the intrinsic carbon property that controls

efficient catalyst deposition on these advanced durable carbon supports. Further, to arrive at a high performance MEA for transportation applications with catalysts on durable carbon supports such as C4, significant effort has to be dedicated towards MEA optimization and fabrication process parameters. Based on the MEA optimization that was attempted under this program for a 20% $Pt_2IrCr/C4$, it is concluded that although stable towards corrosion, Pt-alloy/C4 MEA fabricated using current methodologies and process controls is not expected to meet performance requirements necessary for stack operation.

**Core-Shell Catalysts**

A series of Pt monolayer core shell materials have been successfully prepared using scaleable chemistries, on a range of core types, including $Pd_3Co$, $Pd_3Fe$ and Ir cores. Characterisation of these materials by assay, XRD, HAADF TEM/EELs and in the RDE show successful deposition of a Pt monolayer and properties matching the model systems made at microgram to 2 g scales at BNL.

Much lower activities were observed in MEAs than in the RDE for the $Pt_{ML}/Pd_3Co$ and $Pt_{ML}/Pd_3Fe$ systems. A direct comparison of $Pt_{ML}/Pd_3Co$ materials prepared by JMFC chemical Pt deposition and BNL electrochemical Pt deposition showed equivalent behaviour and ruled out the Pt coating method as a source of the low MEA performances. Detailed measurements of Pd dissolution during electrochemical cycles in liquid electrolytes (i) 0.1M $HClO_4$, room temperature RDE conditions and (ii) 1M $H_2SO_4$, 80°C (analogous to MEAs) showed substantially higher Pd dissolution in the MEA environment and this is thought to be the cause of low performances in MEAs (owing to a mixed Pt/Pd surface under oxidising conditions). Pd dissolution from within the core of a Pt/Pd core shell under oxidising MEA conditions is supported by recent publications[19] and also by modelling work on $Pt_{ML}/Pd_3X$[20] indicating segregation of Pd and X to the surface in the presence of adsorbed oxygen.

Application of various procedures to the $Pt_{ML}/Pd_3Co$ system such as improved reduction, acid leaching or Pd/Ir ion wash treatment of the precursor cores prior to Pt coating did not improve either MEA performance or reduce Pd dissolution. Thus, the high activity of this novel catalyst type, as indicated by RDE activity testing under more benign conditions, could not be realised in MEAs.

The use of the more stable Ir cores translated to improved stability in the $Pt_{ML}/Ir$ core shell and acceptable performance in MEAs. However, no cost benefit is achieved over Pt only on an A/mgPGM basis.

The significant differences in behaviour of $Pt_{ML}/Pd_3Co$ in the RDE and MEA environments cast doubts on the usefulness of the RDE as predictive tool for the stability of catalyst materials. It is also clear that the high activity and good durability of core-shell catalysts reported by the fuel cell community must be treated with caution when results are presented in the absence of MEA testing under realistic operation conditions.

**Molecular Modeling**

a. Model description, key assumptions, version, source and intended use:
   The catalysts were modeled by metallic slabs. The slab model was constructed from a (111) surface unit cell and consists of n-layers of metal atoms and ~n+1 equivalent layers of vacuum (n =6 to10 depending on the system). The metal atoms in the top three (or more, depending on the case) layers were allowed to relax, while the atoms of the bottom layers are fixed to their optimized positions. The geometry of the adsorbates was also fully optimized when they are involved in surface adsorption. In order to measure the segregation trend of the alloy systems, the composition of the top three layers were varied by exchanging the positions of the corresponding metal atoms. The segregation trend was evaluated by the segregation energy, which is defined as the difference of total energies of the slab with metal segregation and that without segregation. Other properties such as stability of the surface

atoms, d-band center, electronic charges, are obtained from the same model. The program **VASP 4.7**[21] was used in all cases.

b. Performance criteria for the model related to the intended use:
Adsorption and segregation energies were compared to reported theoretical and experimental results and trends when available.

c. Test results to demonstrate the model performance criteria were met (e.g., code verification/validation, sensitivity analyses, history matching with lab or field data, as appropriate);
The results obtained under this program were reported in various peer-reviewed articles where the appropriate comparisons to literature results are explained and cited. [17,21,22,23,24,25,26]

d. Theory behind the model, expressed in non-mathematical terms:
The metal catalyst + adsorbates are evaluated in their complete (atomic +electronic) structure. The fundamental laws of physics are solved to determine the electronic density distribution in the system, and that result allows us to evaluate the rest of the thermodynamics and kinetic parameters associated with the system.

e. Mathematics to be used, including formulas and calculation methods;
Mathematics of the basic theory used here: density functional theory (DFT) has already been developed by others and is well-known and reproduced in physics and chemistry textbooks. For a reference, please see "Density Functional Theory: A Practical Introduction" by David Sholl and Janice Steckel, Publishers: John Wiley and Sons. [22]
Other derivations done at TAMU were peer reviewed and reported in a series of published articles. [20,27,28,29,30,31,32,33,34,35,36,37,16]

f. Summary of theoretical strengths and weaknesses;
As explained in (e), DFT methods and mathematical algorithms have been published by others. Modeling results of work performed under this program were published in peer-reviewed articles.[3-15]

g. Hardware requirements;
VASP program normally requires supercomputers. Supercomputing facilities at Texas A&M University, Brazos cluster at TAMU, TACC (University of Texas at Austin), and the supercomputers at NERSC (DOE facility at LBNL, Berkeley) were used for this project.

h. Documentation (e.g., users guide, model code):
Documentation about VASP is available from their developers. [38]

**PATENTS ISSUED/INVENTION DISCLOSURES**

| File Number | Invention Disclosure Title | Date Created | UTC Final Disposition |
|---|---|---|---|
| ID-0006903-US | Reducing Pt particle migration and sintering in fuel cell catalyst by post-deposition of Ir, Pd or Rh | 7-Sep-07 | No Patent |
| ID-0013180-US | AM Texas No. 3044-Dissolution-Resistant Allowy Electrocatalyst for Oxygen Reduction in Acid Medium | 22-Dec-09 | No Patent |
| ID-0015265-US | Method for Synthesis of Electrocatalysts with Very Low Pt Content for PEMFC | 3-Aug-10 | No Patent |
| ID-0016323-US | Hydrophobic treatment of catalyst prior to ionomer-ink formation | 5-Nov-10 | **Patent*** |
| ID-0017471-US | Structure of Cathode Catalyst Layer for High Performance in a WTP PEM Fuel Cell | 28-Jun-11 | No Patent |
| ID-0017719-US | Hydrophobic Channels in the CL of a PEMFC Cathode | 15-Apr-11 | **Patent*** |
| ID-0018633-US | Electrode Fabrication with Well Mixed Catalyst Inks | 7-Jul-11 | No Patent |
| ID-0018697-US | Core-shell Synthesis via Cu ELD method | 8-Jul-11 | No Patent |
| ID-0019463-US | Rib Channel Width Patterned Electrode MPL and GDL for PEM Fuel Cell Performance | 22-Sep-11 | No Patent |

***Application in progress***

## PUBLICATIONS/PRESENTATIONS

1. Ramirez-Caballero, G. E. and Balbuena, P. B. "Surface segregation of core atoms in core-shell structures," *Chem. Phys. Lett*., (**2008**), 456, 64.
2. Ma, Y.; Balbuena, P. B.; Surface segregation in bimetallic $Pt_3M$ (M = Fe, Co, Ni) alloys with adsorbed oxygen, *Surf. Sci*., (**2009**), 603, 349.
3. Murthi, V. S.; Izzo, E.; Bi, W.; Aindow,T. T.; Perez-Acosta, C.; Motupally, S. "Structure-activity-durability relationship of Pt and Pt based alloy electrocatalysts", 215th meeting of the Electrochemical Society, San Francisco, CA, (**2009**). Abstract No. 567
4. Ma, Y. and Balbuena, P. B. "Role of Iridium in Pt-based alloy catalysts for the ORR: Surface adsorption and stabilization studies", *J. Electrochem. Soc*., (**2010**), 157, B959.
5. Ma, Y. and Balbuena, P. B. Surface adsorption and stabilization effect of Iridium in Pt-based alloy catalysts for PEM fuel cell cathodes, Transactions – 216th meeting of the Electrochemical Society, Vienna, Austria; (**2009**), 25, 1, 1037.
6. Ball, S.; Burton, S. L.; Christian, E.; Davies, A.; Fisher, J.; O'Malley, R.; Passot, S.; Tessier, B.; Theobald, B. R. C. and Thompsett, D.; Activity and Stability of Pt Monolayer Core Shell Catalysts, Transactions – 216th meeting of the Electrochemical Society, Vienna, Austria; (**2009**), 25, 1, 1011.
7. Ball, S.; Burton, A.; Fisher, J.; O'Malley, Tessier, B.; Theobald, B. R. C.; Thompsett, D.;Zhou, W. P.; Su, D.; Zhu, Y. and Adzic, R.; Structure and Activity of Novel Pt Core-Shell Catalysts for the Oxygen Reduction Reaction, Transactions – 216th meeting of the Electrochemical Society, Vienna, Austria; (**2009**), 25, 1, 1023.
8. Ramirez-Caballero, G. E.; Ma, Y.; Callejas-Tovar, R.; Balbuena, P. B. "Surface segregation and stability of core-shell alloy catalysts for oxygen reduction in acid medium," *Phys. Chem. Chem. Phys*., (**2010**), 12, 2209.
9. Martinez De La Hoz, J. M.; Callejas-Tovar, R. and Balbuena, P. B. "Size effect on the stability of Cu-Ag nanoalloys," *Mol. Sim*. (**2009**), 35, 785.
10. Gong, K.; Chen, W.; Sasaki, K.; Su, D.; Vukmirovic, M. B.; Zhou, W.; Izzo, E. L.;Perez-Acosta, C.; Hirunsit, P.; Balbuena, P. B.; Adzic, R. R. "Platinum Monolayer Electrocatalysts: Improving the Activity for the Oxygen Reduction Reaction with Palladium Interlayer on IrCo Alloy Core", *J. Electroanal. Chem.* (**2010**), 649, 232.
11. Sarah Ball, "Activity and Stability of Core-shell Electrocatalysts" **2010** Gordon Research Conference in Fuel cells.
12. W. Bi, E. Izzo, V. Murthi, C. Perez-Acosta, J. Lisitano, and L. Protsailo, "Durability of Low Temperature Hydrogen PEM Fuel Cells with Pt and Pt Alloy ORR Catalysts" 218th ECS Meeting - Las Vegas, NV, (**2010**)
13. Martinez de la Hoz, J. M.; Leon-Quintero, D. F.; Hirunsit, P; and Balbuena, P. B.; "Evolution of a Pt (111) surface at high oxygen coverage in acid medium," *Chem. Phys. Lett*., (**2010**) 498, 328.

Acronyms

| | |
|---|---|
| BNL | – Brookhaven National Laboratory |
| BOL | – Beginning of Life |
| CCM | – Catalyst Coated Membrane |
| DFT | – Density Functional Theory |
| ECA | – Electrochemical Area |
| EDAX | – Energy Dispersive X-ray spectroscopy |
| EMPA | – Electron Micro Probe Analysis |
| EOL | – End of Life |
| EW | – Equivalent Weight |
| FT-IR | – Fourier Transform Infra Red |

GDL – Gas Diffusion Layer
JMFC – Johnson Matthey Fuel Cells
KB – Ketjen Black carbon
MA – Mass Activity
MEA – Membrane Electrode Assembly
ML – Mono Layer
ORR – Oxygen Reduction Reaction
PGM – Platinum Group Metal
RDE – Rotating Disk Electrode
RH – Relative Humidity
SP – Solid Plate
TAMU – Texas A&M University
TEM – Transmission Electron Microscopy
UTC – United Technologies Corporation
VASP – Vienna Ab initio Simulation Package
WTP – Water Transport Plate
XAS – X-ray Absorption Spectroscopy
XRD – X-ray Diffraction

**REFERENCES**

[1] S. Mukerjee, S. Srinivasan, M. P. Soriaga, and J. McBreen, *J. Electrochem. Soc*., 142, 1409 (**1995**).
[2] S. Mukerjee, S. Srinivasan, M.P. Soriaga, and J. McBreen, *J. Phys. Chem. A*, 99, 4577 (**1995**).
[3] U. A. Paulus, A. Wokaun, G. G. Sherer, T. J. Shmidt, V. Stamenkovic, V. Radmilovic, N. M. Markovich, and P. N. Ross, *J. Phys. Chem. B*, 106, 4181 (**2002**).
[4] J. Zhang, Y. Mo, M. B. Vukimirovic, R. Klie, K. Sasaki, and R. R. Adzic, *J. Phys. Chem. B*, 108, 10955 (**2004**).
[5] E. Antolini, J. R. C. Salgado, and E. R. Gonzalez, *J. Power Sources*, 160, 957 (**2006**).
[6] Q. Huang, H. Yang, Y. Tang, T. Lu, and D. L. Akins, *Electrochem. Comm*., 8, 1220 (**2006**).
[7] V. R. Stamenkovic, B. Fowler, B. S. Mun, G. Wang, P. N. Ross, C. A. Lucas, N. M. Marković, *Science*, 315, 493 (**2007**)
[8] L. Protsailo, DOE Annual report (**2005**) "Development of High Temperature and Advanced Cathode Catalysts", UTCFC DE-FC36-02AL67608.
[9] J. Zhang, M. B. Vukmirovic, K. Sasaki, F. Uribe and R. R. Adzic, *J. Serb. Chem. Soc*., 70, 513 (**2005**).
[10] M. B. Vukmirovic, J. Zhang, K. Sasaki, A. U. Nilekar, F. Uribe, M. Mavrikakis and R. R. Adzic, *Electrochim. Acta*, 52, 2257 (**2007**).
[11] M. Shao, K. Sasaki, N. S. Marinkovic, L. Zhang and R. R. Adzic, *Electrochem. Comm*., 9 2848, (**2007**).
[12] V. S. Murthi, DOE Hydrogen Program Annual Progress Report (**2010**)
[13] S. Motupally, DOE Merit Review Presentation, June 10 **2008**, Washington DC
[14] V. Stamenkovic, T. J. Schmidt, P. N. Ross, N. M. Markovic, *J. Phys. Chem. B* 106**,** 11970 (**2002**).
[15] Y. Ma, and P. B. Balbuena, "Surface segregation in bimetallic $Pt_3M$ (M = Fe, Co, Ni) alloys with adsorbed oxygen", *Surf. Sci*., 603, 349 (**2009**).
[16] R. Callejas-Tovar and P. B. Balbuena, "Oxygen adsorption and surface segregation in (211) surfaces of Pt (shell)/M (core) and $Pt_3M$ (M=Co, Ir) alloys", *Surf. Sci*., 602, 3531 (**2008**).
[17] Ramirez-Caballero, G. E.; Ma, Y.; Callejas-Tovar, R.; Balbuena, P. B.: Surface segregation and stability of core-shell alloy catalysts for oxygen reduction in acid medium. *Phys. Chem. Chem. Phys., 12,* 2209 (**2010**).

[18] V. S. Murthi, DOE Hydrogen Program Annual Progress Report (**2009**).

[19] K. Sasaki, H. Naohara, Y. Cai, Y. M. Choi, P. Liu, M. B. Vukmirovic, J. X. Wang, and R. R. Adzic, *Angewandte Chemie Intl. Ed.*, 49**,** 8602, (**2010**).

[20] Ramirez-Caballero, G. E.; Ma, Y.; Callejas-Tovar, R.; Balbuena, P. B. "Surface segregation and stability of core-shell alloy catalysts for oxygen reduction in acid medium," Phys. Chem. Chem. Phys., (2010), 12, 2209.

[21] Hafner, J.; Furthmuller, J.: VASP, Vienna Ab initio Simulation Program. Austria, Vienna (**2004)**

[22] Sholl, D. S.; Steckel, J. A.: *Density functional theory: A practical introduction*; Wiley: New Jersey, (**2009**).

[23] Ma, Y.; Balbuena, P. B.: Kinetic model of surface segregation in Pt-based alloys. *J. Chem. Theory Comput.*, *4*, 1991 (**2008**).

[24] Ma, Y.; Balbuena, P. B.: Surface segregation in bimetallic $Pt_3M$ (M = Fe, Co, Ni) alloys with adsorbed oxygen. *Surf. Sci*., *603*, 349 (**2009**).

[25] Martinez De La Hoz, J. M.; Callejas-Tovar, R. and Balbuena, P. B. "Size effect on the stability of Cu-Ag nanoalloys," *Mol. Sim*., 35, 785 (**2009**).

[26] Ma, Y.; Balbuena, P. B.: Surface properties and dissolution trends of $Pt_3M$ alloys in the presence of adsorbates. *J. Phys. Chem. C*, *112*, 14520 (**2008**).

[27] Ma, Y.; Balbuena, P. B.: Pt-surface segregation in bimetallic $Pt_3M$ alloys: A density functional theory study. *Surf. Sci.*, *602*, 107 (**2008**).

[28] Ma, Y.; Balbuena, P. B.: Kinetic model of surface segregation in Pt-based alloys. *J. Chem. Theory Comput.*, *4*, 1991 (**2008**).

[29] Ma, Y.; Balbuena, P. B.: Surface segregation in bimetallic $Pt_3M$ (M = Fe, Co, Ni) alloys with adsorbed oxygen. *Surf. Sci*., *603*, 349 (**2009**).

[30] Ramirez-Caballero, G. E.; Balbuena, P. B.: Surface segregation of core atoms in core-shell structures. *Chem. Phys. Lett.*, 456, 64 (**2008**).

[31] Hirunsit, P.; Balbuena, P. B.: Stability of Pt monolayers on Ir-Co cores with and without a Pd interlayer. *J. Phys. Chem. C*, *114*, 13055 (**2010**).

[32] Hirunsit, P.; Balbuena, P. B.: Surface atomic distribution and water adsorption on PtCo alloys. *Surf. Sci.*, *603*, 911(**2009**).

[33] Martinez-DeLaHoz, J. M.; Leon-Quintero, D. F.; Hirunsit, P.; Balbuena, P. B.: Evolution of a Pt(111) surface at high oxygen coverage in acid medium. *Chem. Phys. Lett.*, *498*, 328(**2010**).

[34] Balbuena, P. B.; Callejas-Tovar, R.; Hirunsit, P.; de la Hoz, J. M. M.; Ma, Y.; Ramirez-Caballero, G. E.: Evolution of Pt and Pt-Alloy Catalytic Surfaces Under Oxygen Reduction Reaction in Acid Medium. *Top. Catal.*, *55*, 322 (**2012**).

[35] Ma, Y.; Balbuena, P. B.: Surface properties and dissolution trends of $Pt_3M$ alloys in the presence of adsorbates. *J. Phys. Chem. C*, *112*, 14520 (**2008**).

[36] Ma, Y. G.; Balbuena, P. B.: Role of Iridium in Pt-based Alloy Catalysts for the ORR: Surface Adsorption and Stabilization Studies. *J. Electrochem. Soc.*, *157*, B959 (**2010**).

[37] Gong, K. P.; Chen, W. F.; Sasaki, K.; Su, D.; Vukmirovic, M. B.; Zhou, W. P.; Izzo, E. L.; Perez-Acosta, C.; Hirunsit, P.; Balbuena, P. B.; Adzic, R. R.: Platinum-monolayer electrocatalysts Palladium interlayer on IrCo alloy core improves activity in oxygen-reduction reaction. *J. Electroanal. Chem.*, *649*, 232 (**2010**).

[38] Kresse, G.; Furthmuller, J.: Efficient iterative schemes for ab initio total-energy calculations using a plane-wave basis set. *Phys. Rev. B*, *54*, 11169 (**1996**).